REVIEW ARTICLE

Check for updates

Headway towards contemporary 2D MXene-based hybrid electrodes for alkali-ion batteries

Helen Treasa Mathew,[a] Kumar Abhisek,[a] Shashikant Shivaji Vhatkar[a] and Ramesh Oraon (ID) *[ab]

Recent studies have revealed that the current consumption rate of fossil fuels may lead to their exhaustion in the coming years. Due to the depletion of non-renewable energy sources and the fitness of renewable energy sources, energy storage and management can be viewed as a prime requisite. The inception of advancements in energy storage techniques and rechargeable batteries has eased the problem to a certain extent. With highly exceptional properties such as inherent volumetric capacitance, outstanding conductivity, durability, low energy barriers for metal ion diffusion and the presence of surface functional groups, MXenes have entered the field of energy storage. MXenes are 2-D layers of transition metal carbides or nitrides, synthesized by the selective etching of aluminium from layered MAX phases. The large interlayer spaces for ion intercalation permits alkali ions in these layers, revealing unexpected properties that can be exploited for energy storage in alkali-ion batteries (AIBs) such as lithium/sodium/potassium/magnesium/calcium ion batteries. Electrochemical energy storage can also be visualised as a clean energy storage system. This review covers the synthesis of MXenes, their eminent properties and the fabrication of MXene-based nanomaterials and hybrids for electrochemical energy storage in various alkali-ion batteries. Finally, possible challenges are highlighted for the future exploration of the research possibilities.

[a] Department of Nanoscience and Technology, Central University of Jharkhand, Ranchi, India. E-mail: ramesh.oraon@cuj.ac.in

[b] Department of Chemistry, Central University of Jharkhand, Ranchi, India

1. Introduction

Sustainable energy utilisation is vital since the consumption of resources for our present needs should be established without compromising the needs of future generations. Maximising the efficiency of the energy storage devices and the subsequent

Ms Helen Treasa Mathew received her bachelors' and masters' degree from Mahatma Gandhi University and Kannur University Kerala, India in 2018 and 2020, respectively. She has worked as project trainee in ESMB Division of CSIR-NPL, New Delhi. Currently, she is pursuing PhD from the Department of Nanoscience and Technology, Central University of Jharkhand, India. Her research interest is in the synthesis and modification of MXene-based hybrid materials for multifarious applications.

Helen Treasa Mathew

Mr Kumar Abhisek obtained his masters' degree from NIST, Berhampur, Odisha, India in 2020, and pursuing PhD in Department of Nanoscience and Technology, Central University of Jharkhand, India. He is currently working on the development of transition metal dichalcogenide-based multifunctional hybrid materials for environmental applications.

Kumar Abhisek

utilisation of best available technologies to harvest renewable energy would lead to fully sustainable global energy systems.[1–3] In addition to sustainability, efficient energy storage systems can pave the way towards the reduced usage of fossil fuels thereby remediating environmental pollution.[4–6] Such a scenario can be achieved through suitable electrochemical energy storage devices.[7,8] Among the many such devices, lithium-ion batteries (LIBs), with high energy density, limited self-discharge, long wheel-of-life and environmental amiability have become more popular.[9,10] The reduced availability of naturally occurring Li and economic feasibility hinder the further enhancement of these batteries to a certain extent.[11,12] However, an alternative is needed to meet the requirements for suitable storage devices. Sodium and potassium have similar properties as Li and could easily alleviate the disadvantages due to their natural abundance and lower supply cost. Both sodium-ion batteries (SIBs) and potassium-ion batteries (PIBs) suffer from low reversible capacity and poor cycling stability due to low open circuit voltages and large ionic radii, making it harder to find a suitable host.[13,14] Multivalent alkali metal-ion batteries such as magnesium-ion batteries (MIBs) and calcium-ion batteries (CIBs) have been advantageous due to their low price, abundant resources and high safety applications.[11,15,16] Moreover, all alkali metal batteries are susceptible to dendrite growth, which will adversely intensify their electrochemical performance and cause a safety hazard.[17,18] To satisfy the requirements, electrode materials are expected to have desirable electron or ion conduction, physicochemical properties, excellent electrochemical performance and structural stability during repeated charge/discharge cycles.[19,20] To meet these requirements, diligent efforts have been made to investigate and establish suitable nanomaterials for advanced electrodes in alkali-ion batteries.

Interestingly as a solution to all the above-mentioned problems, MXenes, a new family of compounds, have emerged, in which alkali and non-alkali ions can be intercalated. MXenes are a 2D group of early transition metal carbides and/or carbonitrides, produced by the etching out of the A layers from MAX phases.[21] The MAX phases are composed of an early transition metal M, a group 13 or 14 element denoted as A and C and/or N denoted as X, forming $M_{n+1}AX_n$, where $n = 1, 2,$ or 3. Among the different family groups of MAX phases, more than 130 possess the MX_6 octahedral structure.[22] At the initial stage, almost 50 MAX phases were discovered.[23] The number of M layers found between A layers differs from one type to another, namely the 211, 312 or 413 phases.[24] In 2014, B. Ansori *et al.* synthesised a new chemically ordered ternary carbide, Mo_2TiAlC_2, in which Ti layers are sandwiched between two Mo layers.[25] Later, in 2017, Liu *et al.* developed other ordered MAX phases $(Cr_{2/3}Ti_{1/3})_3AlC_2$ and $(Cr_{5/8}Ti_{3/8})_4AlC_3$.[26] These were out-of-the-plane or o-MAX 312 or 412 phases. However, the 2D $Mo_{1.33}C$ sheets, which possessed high conductivity and volumetric capacitance, were in-plane ordered or i-MAX 211 phase.[27] Bond structures of the MAX phases are strong enough so that they cannot be broken by any mechanical means like stress or shear. Yet, the differences in the relative strengths of the M–A and M–X bonds permit the selective etching of A layers from M–A bonds without disturbing the M–X bonds.[28] Thereby, 2D MXenes are characterised by the formula $M_{n+1}X_nT_x$, where T represents the functional groups getting adsorbed at the surface of MXenes and x means the number of surface functionalities.[29] Alterations made in the interlayer spacing of MXenes, without disrupting the layered structure, promote the synthesis of MXenes-based composites with outstanding performance. In addition to that, the properties such as electronegativity, hydrophilicity and surface structure tunability of the adsorbed terminations show up without affecting the conductivity.[30]

According to theoretical calculations MXenes and MXene-based electrodes, possess low ion-diffusion barriers, specific capacity, cyclability and appreciable conductivity. This in turn enhances the electrochemical performance of these alkali-ion batteries.[31–33] Furthermore, MXene-based materials that inhibit the growth of metal dendrites also encourage research enthusiasm towards the manufacture of high-performance electrodes. The incorporation of MXenes with heteroatoms,

Shashikant Shivaji Vhatkar

Mr Shashikant Shivaji Vhatkar is pursuing his PhD in the Department of Nanoscience and technology from Central University of Jharkhand, Ranchi, India. He received his masters' from Central University of Tamil Nadu, India majoring in materials science in 2018. He has been working on development and electrochemical study of polyindole-based hybrid electrode materials for energy storage applications.

Ramesh Oraon

Dr Ramesh Oraon is presently working as an assistant professor in Department of Nanoscience and technology (now Dept. of Chemistry) since 2018. He obtained his bachelors' from St. Xavier's college, Ranchi, Jharkhand, India in 2010. He received his masters and PhD from IIT-ISM Dhanbad in 2012 and 2017 respectively. He has been actively involved in developing hybrid electrode materials and their electrochemical study for energy storage and environmental applications.
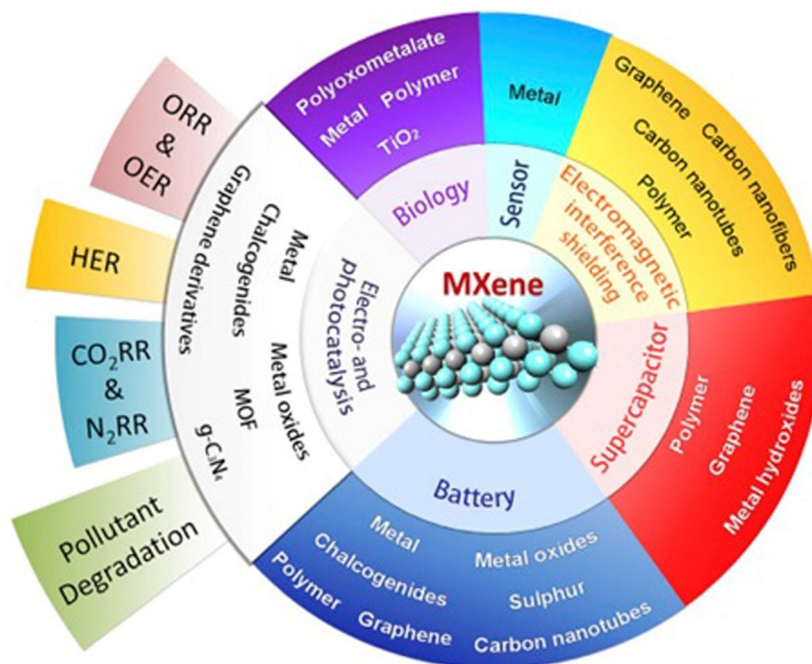
Fig. 1 MXene-based hybrid electrode materials and their diverse applications. This figure has been reproduced/adapted from ref. 37 with permission from Elsevier Inc.

CNTs or other nanostructures forms MXene-based hybrids that enhance the electrochemical performance of the cathode/anode materials. It was shown that alkalization transforms MXenes into 3D nanoribbons and they have been applied to PIBs, SIBs and LSBs to obtain dendrite-free electrode materials.

The development of suitable composites can elevate their exploration in different fields as depicted in Fig. 1. By inducing suitable morphological modification and with appropriate functionalisation, MXenes work as an intriguing interface in various sensing applications since they possess strong metallic conductivity, hydrophilicity, low diffusion barrier, high ion transport characteristics and large surface areas.[34] They are utilised in physical sensing, which includes the sensing of stress, strain or pressure, and chemical sensing, which comprises gas sensing as well as biosensing.[35] Wang et al. developed hybrid MXene/ZnO nanorods for NO_2 sensing, which exhibited higher sensing capability than the pristine ZnO rods at ambient temperature.[36]

Ultra-thin, flexible MXene-based materials can be utilised for electromagnetic interference (EMI) shielding, owing to their exceptional conductivity, lightweight nature, easy producibility, as well as large surface area.[38] Apart from these applications, they are employed in supercapacitors because they have extraordinary physical and electrochemical characteristics and their composition can be tuned accordingly.[39] Interestingly, MXene-based hybrid materials are used as photocatalysts as they might enable quick photoinduced separation of charge carriers in photocatalytic activity and offer many surface functionalities for materials used for light-harvesting, ensuring the possibility of achieving high photoconversion efficiencies.[40] 2D MXene-based nanomaterials have a myriad of very desirable

characteristics, including rich surface functionalities, excellent conductivity, changeable bandgap architectures, hydrophobicity, a sizable surface area and thermal stability. When used with various sophisticated oxidation techniques for the breakdown of hazardous contaminants, MBNs function as an exemplifiable alternative.[41] Additionally, there is considerable interest in investigating the potential of MXenes to be introduced at the interfaces of biological systems due to their dimensionality, large effective surface area, planar shape and surface chemistry, along with favourable physicochemical features.[42]

In this review, we initially focus on various bottom-up and top-down synthesis methods for MXenes and their outstanding properties that make them dominant in the field of energy storage applications. This review highlights the development of different electrodes that may use MXenes, heteroatom-doped MXenes, or MXene-based hybrids/composites as hosts to enhance the performance of lithium-ion batteries and non-lithium-ion batteries. Also, we cover the synthesis of high-performance lithium-based batteries like lithium–metal batteries (LMBs), lithium–air batteries (LABs) and lithium–sulphur batteries (LSBs). Finally, we set forth the hurdles and challenges for the synthesis of dendrite-free, high-capacity MXene-based electrodes and unveil the possible horizons for MXene materials for future research.

2. Synthesis of MXenes

MXenes are derived by the selective etching of definite atomic layers of the precursor MAX phase, which are a group of ternary

Table 1 A glimpse at the MXenes synthesised to date

Precursors	MXenes synthesised	Etchants used	Synthesis parameters		Ref.
			Temperature (°C)	Reaction time (h)	
Ti_2AlC	Ti_2CT_x	10% HF	RT	10	47
V_2AlC	V_2CT_x	50% HF	RT	90	48
Nb_2AlC	Nb_2CT_x	50% HF	RT	90	49
Ti_2AlN	Ti_2NT_x	5% HF	RT	24	50
Mo_2Ga_2C	Mo_2CT_x	50% HF	50	3	51
$(Ti_{0.5}Nb_{0.5})_2AlC$	$(Ti_{0.5}Nb_{0.5})_2CT_x$	51% HF	RT	28	52
Ti_3AlC_2	$Ti_3C_2T_x$	50% HF	RT	2	53
$(V_{0.5}Cr_{0.5})_3AlC_2$	$(V_{0.5}Cr_{0.5})_3C_2T_x$	50% HF	RT	69	52
Ta_4AlC_3	$Ta_4C_3T_x$	50% HF	RT	72	52
Nb_4AlC_3	$Nb_4C_3T_x$	50% HF	RT	96	54
V_4AlC_3	$V_4C_3T_x$	40% HF	RT	165	55
Ti_3AlCN	Ti_3CNT_x	30% HF	RT	18	52
Mo_2TiAlC_2	$Mo_2TiC_2T_x$	50% HF	RT	48	56
$Mo_2Ti_2AlC_3$	$Mo_2Ti_2C_3T_x$	50% HF	55	90	57
$(Mo_{2/3}Y_{1/3})_2AlC$	$Mo_{4/3}CT_x$	48% HF	RT	60	58
$(Mo_{2/3}Y_{1/3})_2AlC$	$Mo_{4/3}CT_x$	10% HF	RT	72	58
$(Nb_{2/3}Sc_{1/3})_2AlC$	$Nb_{4/3}CT_x$	48% HF	RT	30	59
$(W_{2/3}Sc_{1/3})_2AlC$	$W_{4/3}CT_x$	48% HF	RT	30	60
$Zr_3Al_3C_5$	$Zr_3C_2T_x$	50% HF	RT	60	61
$Hf_3[Al(Si)]_4C_6$	$Hf_3C_2T_x$	35% HF	RT	60	62
Ti_2AlC	Ti_2CT_x	0.9 M LiF + 6 M HCl	40	15	63
Mo_2Ga_2C	Mo_2CT_x	3 M LiF + 12 M HCl	35	384	64
V_2AlC	V_2CT_x	2 g LiF + 40 M HCl	90	48	65
Ti_3AlC_2	$Ti_3C_2T_x$	3 M LiF + 6 M HCl	40	45	66
Ti_3AlCN	Ti_3CNT_x	0.66 g LiF + 6 M HCl	35	12	67
Cr_2TiAlC_2	$Cr_2TiC_2T_x$	5 M LiF + 6 M HCl	55	42	56
$(Nb_{0.8}Zr_{0.2})_4AlC_3$	$(Nb_{0.8}Zr_{0.2})_4C_3T_x$	LiF + 12 M HCl	50	168	68
$(W_{2/3}Sc_{1/3})_2AlC$	$W_{4/3}CT_x$	4 g LiF + 12 M HCl	35	48	60
Ti_3AlC_2	$Ti_3C_2T_x$	1 M NH_4HF_2	80	12	69
Ti_3AlC_2	$Ti_3C_2T_x$	NH_3F	150	24	70
Ti_4AlN_3	$Ti_4N_3T_x$	59% KF + 29% LiF + 12% NaF	550	0.5	71

carbides and nitrides possessing a double transition metal structure. The wedging of the A layers between the M and X layers produces a structure with weak M–A bonds and strong M–X bonds.[28,43] Therefore, utmost care should be taken for the selection of an appropriate, simplistic and harmless method of synthesis that would retain the M–X bonds. This choice is significant because the properties of MXenes are greatly influenced by the etching environments during synthesis.[44] The comparative studies of different MXene-based electrodes reveal that different surface functional groups affect the performance to an extent, as they can be tuned to obtain desired properties. MXenes with surface terminations, bromine and iodine significantly increase the electrochemical performance of the AIBs as compared to chlorine.[45] Unfortunately, the majority of the currently employed synthetic methods yield MXenes that are surface halogenated with Cl and F. In addition to that, the morphology, internal defects and yields of the synthesised MXenes are strongly influenced by experimental factors like the concentration of the etchant, temperature, and time taken for synthesis, *etc.* Nan *et al.* reported that these defects in MXenes tend to react with active cations, which may further lead to batteries with poor first coulombic efficiency.[46] Hence, before the detailed analysis, sufficient knowledge of the synthesis of MXenes is requisite. In general, MXenes can be synthesised either by top-down or bottom-up techniques (Table 1).

2.1 Top-down techniques

These techniques involve the depilation of the precursor MAX phases to form MXenes.[72] The precursor for this method is the Al-containing MAX phases that have given rise to more than 30 MXenes to date and they inherit the structural ordered features of their corresponding MAX phases.[28] After the selection of a suitable precursor, it is exposed to etching, which can be done by using fluoride-carrying aqueous solutions, molten-salt etching, or by alkaline/hydrothermal treatments. High-temperature etching can give rise to 3-D phases, and hence low-temperature methods are promoted for the formation of 2D structures.[73] Once etching is done, due to the large numbers of cations and organic molecules present within these multilayers, suitable molecules have to be brought in to separate them into single nanosheets. These by-products are washed away by the process of sonication or shaking with liquid molecules. If it is done by HCl/LiF, direct sonication cannot be applied.[74,75] The most commonly used polar organic molecule for exfoliating Ti_3AlC_2 is dimethyl sulfoxide (DMSO).[76,77] The position of (0002) peaks in the XRD pattern represents the interlayer *d*-spacing of 9.8 Å. The co-instantaneous intercalation of DMSO and water results in the inflation of the *d*-spacing to about 22.4 Å.[77] This sonication process can also be carried out with a solution of tetra-butylammonium hydroxide (TBAOH).[78] The intercalation of TBA ions into the layers will be enhancing the interlayer distance greatly and therefore, this method is most commonly
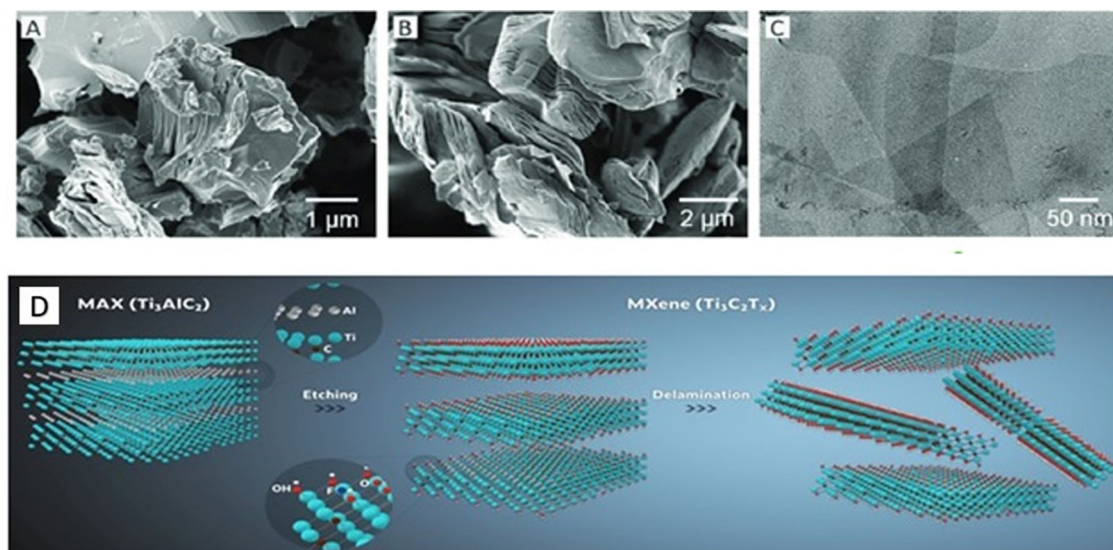
Fig. 2 SEM micrographs of (A) the Ti$_3$AlC$_2$ MAX phase and (B) Ti$_3$C$_2$T$_x$ multi-layered MXene. (C) The TEM micrograph of the overlapping MXene layers. This figure has been reproduced/adapted from ref. 79 with permission from Elsevier Inc. (D) A schematic diagram of the etching and delamination of Ti$_3$C$_2$T$_x$ MXene. This figure has been reproduced/adapted from ref. 80 from Chemical Society Reviews 2020.

used for exfoliation purposes. Fig. 2(A) and (B) illustrate the SEM and (C) TEM micrographs obtained during the top-down synthesis scheme of Ti$_3$C$_2$T$_x$ MXene from the Ti$_3$AlC$_2$ MAX phase as shown Fig. 2(D).

2.1.1 HF Etching. This is the conventional or oldest method of MXene synthesis, where the powdered MAX phase is submerged in a specifically concentrated aqueous HF solution at a predetermined temperature for a particular period.[81] Selective etching can give rise to multi-layered MXenes, which on sonication yield the desired MXene nanosheets.[82] The concentration of the etchant used, time taken for etching and reaction temperature vary according to the type of metal in the MAX phase, as there is an increase in bond energy with the increase in the atomic number;[21,46] the type of MXene to be synthesised can also alter the etching conditions. Studies have revealed that it is comparatively easier to synthesise transition metal carbides than nitrides.[83] Not all MXenes can be produced by HF etching; however, Ta$_4$C$_3$T$_x$, TiNbCT$_x$, Ti$_3$CN$_x$T$_x$, Nb$_4$C$_3$T$_x$, (Nb$_{0.8}$Zr$_{0.2}$)$_4$C$_3$T$_x$, etc., have been successfully prepared by this method.[56,64,81,84,85] Because the process of HF etching is exothermic, precautions must be taken to control the reaction parameters to avoid hazardous circumstances. On taking an account of the issue, the direct usage of HF can be duplicated by the use of a mixture of fluoride salts and strong acid, which locally forms the HF required for etching.[86] Michael Ghidiu et al. reported the synthesis of MXene with the help of the milder LiF and HCl. The fascinating achievement was the formation of single- or few-layered MXene nanosheets with large interlayer spacing and no interaction, induced by the spontaneous intercalation of cations in metal fluorides and water molecules into the layers during etching, without any additional intercalating reagent.[66] Another method for alleviating the rigorous behaviour of HF is with the aid of

HF-containing NH$_4$HF$_2$. It was used in etching epitaxially developed Ti$_3$AlC$_2$ by Halim et al. in 2014 to obtain MXenes with larger interlayer spacing due to the presence of NH$_3$ and NH$_4^+$ intercalated between the layers.[69] This result is advantageous for the delamination of multilayer MXenes and the introduction of metal ions like Li$^+$, Na$^+$, K$^+$, etc. into these layers.[87] Simon et al. experimented to proclaim that the intercalation of surfactants could control the interlayer spacing, which would, in turn, improve their electrochemical performance.[88] Fig. 3 represents an illustration where MXene foam is generated by the LiF/HCl etching of the Ti$_3$AlC$_2$ MAX phase.

2.1.2 Other top-down methods. Methods for the synthesis of fluorine-free MXenes include molten salt etching, alkali
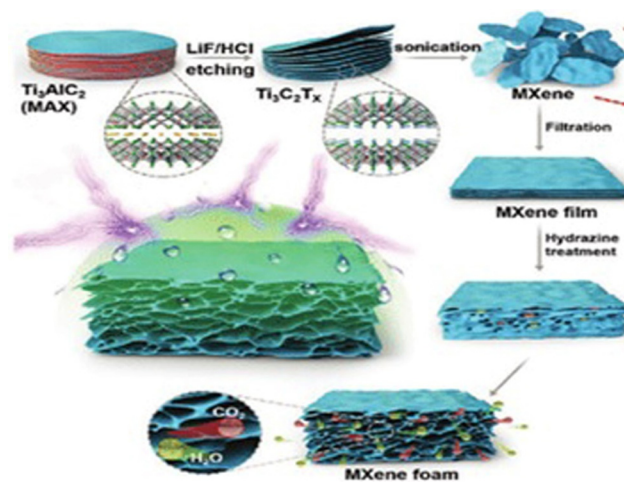

Fig. 3 Schematic representation of the fabrication of a flexible and hydrophobic MXene foam. The image was adapted/reproduced from ref. 89 with permission from Advanced Materials 2017.

etching assisted by high-temperature, and electrochemical etching.[46,86] Even though fluorine has a high affinity towards the A layers of the MAX phase, higher concentrations reduce the MXenes' conductivity, thereby restricting application in energy storage.[90] MXenes prepared by molten salt etching have proved to be efficient in manufacturing negative-electrode materials with a high rating for electrochemical energy storage.[91] One of the viable methods of preparing MXenes deprived of fluorine is by Lewis acid etching. Li et al. used $ZnCl_2$ as a Lewis acid to prepare MXenes that are surface terminated with chlorine from Al-layered MAX phases (Ti_3AlC_2, Ti_2AlC, Ti_2AlN and V_2AlC) in an argon environment at 550 °C for 5 hours.[92,93] The quantity of $ZnCl_2$ should be taken in excess so that the formation of the Zn MAX phase is prevented. However, Zn by-products will be formed and this can be removed by treatment with hydrochloric acid. Later, in 2020, Youbing Li and co-workers synthesised MXenes from Al-containing and Si, Zn, and Ga-containing MAX phases.[94] $CuCl_2$ molten salt was used to etch Ti_3SiC_2 at 750 °C to obtain the corresponding MXene and the Cu formed as a by-product was washed out by $(NH_4)_2S_2O_8$ solution. This increases the electrochemical performance of the MXene as they provide terminations of O and Cl at the surface. Later, O, NH, S, Cl, Se, Br and Te-terminated MXenes were produced by treating them with molten inorganic salts.[95]

Another method used to prepare fluorine-free MXenes is by treating the MAX phases with an alkali solution at a high temperature. If the reaction is conducted without high-temperature conditions, etched Al forms an aluminum oxide or hydroxide layer around the MAX phases, prohibiting further reactions. Li et al. described the etching of Ti_3AlC_2 with a 27.5 M NaOH solution at 270 °C.[93] $Ti_3C_2T_x$ electrodes made free of fluorine showed a higher gravimetric capacitance (314 F g^{-1}), which was 214% more than that made out of HF-etched MXenes.[96]

Electrochemical etching is another method for synthesising MXenes without the utilisation of toxic substances. However, the reaction parameters and requirements must be strictly met to prevent excessive etching. Over-etching can cause the development of a carbon layer over the MAX phase that prevents subsequent etching reactions.[97] Yang et al. prepared MXenes through a controlled lithiation-alloying expansion micro explosion mechanism.[98] In this process, $Ti_3C_2T_x$ MXene layers can be synthesised after lithium intercalation and sonication in water. Lithium intercalation processes give rise to 100% volume expansion. This Al–Li alloy immersed in water reacts to form hydrogen gas by a micro-explosion process, which leads to the formation of exfoliated MXenes nanosheets. The exfoliating process is performed in water, which automatically avoids the usage of toxic etchants.

2.2 Bottom-up synthesis techniques

There are various MXenes with certain stoichiometries that cannot be synthesised through selective etching and they can utilise this method of synthesis. Ultra-thin 2D films with high crystalline quality can be fabricated using bottom-up methods like chemical vapour deposition, the template method, and plasma-enhanced pulsed laser deposition.[79] Single layers are not formed through these methods; instead, thin films of few layers are prepared. Also, the films prepared by this method possess superconductive transitions within.[59]

2.2.1 **Chemical vapour deposition (CVD).** Even though the notable hurdles put forward in HF etching were overcome by the subsequent substitutes, a more suitable and sustainable method called chemical vapour deposition was introduced. Researchers prefer this method because it can regulate the material thickness, which was found to be of great importance.[87,99] Larger-sized MXenes with fewer functional defects can be synthesised by this method. Xu et al. used a copper/transition bilayer metal foil for growing α-Mo_2C crystals by this method.[100] Mo_2C crystals were formed by heating the stack to 1085 °C in hydrogen and then using the methane flow rate. The Cu layer acts as a catalyst to form carbon from methane and also channels the diffusion of Mo atoms to liquid Cu, which eventually forms ultrathin layers. Although these layers were stable and exhibited superconducting transitions, they were a combination of 6 ultrathin layers and not a single MXene nanosheet. The thickness of the Mo_2C crystals was found to be altered by altering the thickness of Cu foil and methane concentration.[101] Polygonal crystals were obtained after the alterations. Wang et al. synthesised Ta-compounds using CVD by heating the tantalum-copper bilayer with the precursor (C_2H_2, B powder, and NH_3).[102] The copper foil was kept in the solid-state and ultrathin TiC, TiN, and TiBr were prepared by using boron instead of ammonia. The thickness of 2D crystals was controlled below the melting temperature of copper.

Although it produces high-quality films, this technique is not suitable for the synthesis of MXenes as they produce thin layers rather than a single layer. Additionally, high production costs and low yields also set forth a hurdle for its further application.

2.2.2 **Other bottom-up methods.** Increasing the yield of production was the core concern in moving from CVD to other techniques. An alternative method used for the preparation of high-yield 2D transition metal carbides and nitrides is the template technique. This method uses 2D transition metal oxide nanosheets, which are further carbonized or nitrified. The structure of the synthesised carbides and nitrides depends upon the type of metal oxide used. This method converts 2D MoO_3 nanosheets by heating ammonia at 800 °C to make 2D hexagonal molybdenum nitride (MoN) nanosheets.[103] These layered 2D MoN nanosheets possess a lateral size of 20–30 μm and a thickness of 5–40 nm, which is thicker than that produced earlier. Another bottom-up method for a similar preparation is the plasma-enhanced pulsed laser deposition method (PEPLD). This method is the integration of chemical vapour deposition and pulsed laser deposition methods. Zang et al. successfully developed continuous Mo_2C ultrathin single-crystalline films by plasma-enhanced pulsed laser deposition.[104] Methane is used as the carbon source; the substrate used is sapphire and is heated at a temperature of

Table 2   Advantages and disadvantages of different MXene synthetic methods[105]

Type of method	Advantages	Disadvantages
HF etching	• Convenient and easy method	• The reaction is highly exothermic and may invite hazardous situations.
	• Produces high-quality MXene layers	• HF can be corrosive/poisonous.
	• Retains the surface properties.	
HCl + fluoride salt etching	• Less toxic than HF	• Time-consuming multi-step synthesis
	• Enhances the cation intercalation	
Molten salt etching	• Fast processing time	• Highly energy-consuming process
	• Produces MXenes of limited stability	• Produces MXenes of poor crystallinity and purity.
		• A large number of vacancies and surface faults.
CVD technique	• Produces high-quality films.	• High production cost and low yields.
	• Regulates the material thickness.	• Produce thin layers rather than a single layer.
	• Sustainable method.	
PEPLD technique	• Produces films that are ultra-thin and continuous.	• Low crystalline quality.
		• A large number of stacking defects.

700 °C. The films formed by PEPLD exhibited low crystalline quality and an increased number of stacking faults prevailed in the films. Advanced measures have to be taken for the improvement of the bottom-up synthesis method of MXenes to make the process more sustainable, non-toxic and productive (Table 2).

3. Characteristic features of MXenes

MXenes, with their versatile physical, chemical, electrical, and magnetic properties, have attracted many researchers to explore the scope for their employment in various applications. As we have already observed, the synthesis environment, the chemistry of the etchant used, the properties exhibited by the corresponding MAX phases and surface terminations are the general factors that influence the properties of MXenes.[106,107] The 2D morphology, ion mobility and electronic transport features make it convenient to fabricate electrodes with expected performances for energy storage. Studies have revealed that Density Function Theory (DFT) has helped to unveil the chemical and physical properties of MXenes.[56] According to DFT, Sc-based MXenes are more semiconductor-like with a free carrier density of $8 \pm 3 \times 10^{21}$ cm^{-3}, mobility of 0.7 ± 0.2 cm^2 V^{-1} s^{-1}, an electrical conductance of 9.5×10^4 S cm^{-1} and Hall carrier mobility of 54.58 cm^2 V^{-1} s^{-1}.[108,109] The first principal study also manifested that Ti-based, alkali-adsorbed MXenes like $Ti_3C_2T_x$ and Ti_2CO_2 were metallic.[110,111]

3.1 Mechanical properties

MXenes exhibit superior flexibility and high mechanical strength. However, the mechanical properties can vary with the number of layers denoted by the letter n in the structural formula of the surface-modified MXenes. M_2X is stronger and more rigid as compared to M_3X and M_4X MXenes as stated by DFT and molecular dynamics.[112,113] The elasticity, optical response, and crystal structure also show strong reliability on the surface terminated groups. Due to the smaller lattice constants, the elastic stiffness of the O-terminated MXenes is predicted to be much higher than F/OH terminated MXenes.[114] Guo et al. explained that surface functional groups form a

buffer layer when Ti$_2$C is exposed to tensile deformation, thereby increasing its resistance towards strain and slowing down the fracture of Ti layers.[115] Kurtogolo et al. explained the smaller modulus of MXene with the help of first principles theory, while Lei et al. presented a decline in the surface modulus and enhancement in the flexibility of MXene as compared with graphene.[112,116] Recent studies have revealed that the formation of composites of MXenes like $Ti_3C_2T_x$–PVA, $Ti_3C_2T_x$–PVA can enhance the mechanical strength and elasticity even more.[70,117]

3.2 Thermal stability

In MXene-based nanomaterials, thermal stability can be viewed as a crucial element as it directly influences the properties, thereby restricting their applications.[118] The type of highly active transition metal, etching agent, surface functionalisation, etc. can affect the stability of MXenes. According to Seredych et al., the thermal stability of $Ti_3C_2T_x$ MXene was comparatively superior to Nb_2CT_x and Mo_2CT_x MXene and can be improved using weak etchants.[119] Absorbed functional groups establish a negative charge on the surface of MXenes and their edges will be positively charged.[120] Hence the oxidation process starts from the edge and grazes into the entire MXene nanosheets. Barsoum et al. declared that polyanions adsorbed at the edge of MXenes nanosheets diminish the oxidation tendency of nanosheets, even if the MXenes are exposed to aerated water for several weeks.[121–123] Because oxidation can deteriorate the properties of MXenes, the proper choice of synthesis methods, and regulating the storage environment and edge capping methods can improve the stability and performance of O-terminated MXenes.[124]

3.3 Adsorption sites and surface functionalisation

There are four prevailing adsorption sites for the functional groups in the MXenes.[125] Firstly, the functional groups can be found on the top of the hollow sites above the metal M ions. Secondly, the functional group can be attached at the top of the hollow sites above the X ions. Thirdly, the functional groups can be directly located on the top of the transition metal (M) ions. Lastly, some of the functional groups located on the top of

the hollow sites above transition metal (M) ions, with other functional groups can be located on the hollow sites of X ions. A comparative study regarding the binding energy of the surfactants O, OH, and F on 2D MXene surfaces was done by Ashton *et al.*[126] A study was conducted to understand the thermodynamic stability of these compounds and their variation in chemical composition. On referring to the thermodynamic stability of all 54 MXene compounds with $M_{n+1}X_nO_2$ (M = Sc, Ti, V, Cr, Zr, Nb, Mo, Hf, Ta; X = C, N; n = 1, 2, 3), 38 were found to have formation energies of 200 meV per atom. Among these 38 compounds, only six are assumed to possess formation energies below 100 meV per atom. However, Sc-based MXenes are highly stable because their surfaces are terminated with F. They can easily produce freestanding single layers that result in the easiest exfoliation.

3.4 Electric and magnetic properties

MXenes are known to be versatile as they exhibit dynamic electrical properties ranging from insulation in the bulk to metallicity, semiconductivity and even superconductivity, which are strongly influenced by surface functionalisation, the precursor MAX phase and etching process.[95,127] The studies on this interesting behaviour by Bansori *et al.* confirmed that the molybdenum-containing MXene, $Mo_2TiC_2T_x$ with OH termination possesses high conductivity, though $Ti_3C_2T_x$ shows metallicity. The synthesis method can also alter the electrical conductivity of the MXenes. The usage of mild etchants and proper delamination can give rise to MXenes with larger-sized flakes and fewer defects, which will automatically increase conductivity.[128] According to first principles calculations, alteration of Fermi levels by surface terminations can change the conductivity of MXenes.[129] Surface terminations induce changes in the work functions of the MXenes. Recent researchers established that OH-terminated MXenes exhibit very low work functions (1.6–2.8 eV), O-terminated ones increase the work function, whereas F-terminated ones increase or decrease it based on the type of material used.[130] Increased electronic transport and conductivity can help MXenes to be deployed in the manufacture of electrode materials for various alkali-ion and metal-ion batteries.

The strong covalent bonding between metal, X element and the terminal group makes pure MXenes non-magnetic. However, when exposed to mechanical strain, the magnetic moments of such non-magnetic MXenes show a transition from zero magnetism to ferromagnetism.[131,132] MXenes can also be combined with suitable compounds to form composites with even better conductivity and magnetoresistance can act as a frontier to the further exploration of MXene application in the field of electrochemical energy storage.

4. MXenes in alkali-ion batteries

MXenes with their prominent electrochemical performance can be used for preparing electrodes for alkali-ion batteries. Lithium–ion batteries have become popular in the field of
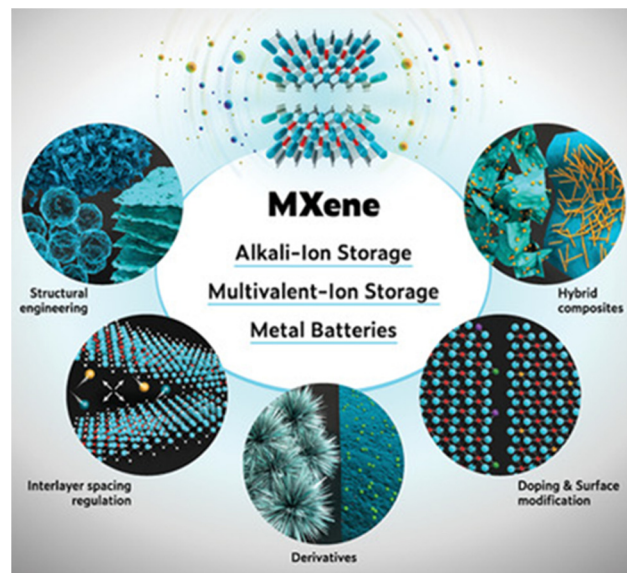

Fig. 4 A pictorial representation of the various methods that can deploy MXenes in non-lithium alkali-ion batteries to enhance their performance rates. The image was adapted/reproduced from ref. 133 with permission from Advanced Materials 2021.

electrochemical energy storage with their high energy density, reliability and cyclability. However, their natural abundance and similar properties to Li have helped Na and K to get employed in energy storage applications. An inevitable challenge to be faced for the large-scale production of SIBs and PIBs is the requirement for electrode materials with large intercalation spaces due to their larger ionic radii. Studies have revealed that surface-functionalized MXenes that can form well-defined composites can meet the requirements for the manufacture of SIBs with advanced storage capacities and low diffusion barriers for sodium.[31,32] Because of the radius of the potassium ion, PIBs can be intercalated within MXenes to form composites to achieve the expected performance.[33] The proper design of electrode materials can improve their storage capacity, electronic transport, and efficiency to improve the performance of LIBs as well as non-LIBs. Fig. 4 illustrates the schematic representation of the measures that can be adopted to enhance the rate of performance in non-lithium AIBs.

4.1 MXenes in lithium-ion batteries

Lithium-ion batteries with their appreciable electrochemical properties can be deemed as the most convincing option for energy storage in portable devices, electric vehicles and forthcoming storage devices.[134] During the initial phase, the conventional $C/LiCoO_2$ electrode used in LIBs, due to the low ability of graphite for intercalation, high cost, toxic nature of Co and $Li_{1-x}CoO_2$ phase thermal stability, was displaced by the $C/LiFePO_4$ configuration. Although the latter solved the affordability and environmental toxicity issues, the energy density was diminished due to reduced operating voltage.[135] The advent of MXenes paved the way towards the manufacture of advanced hybrid electrodes that exhibited outstanding stability,
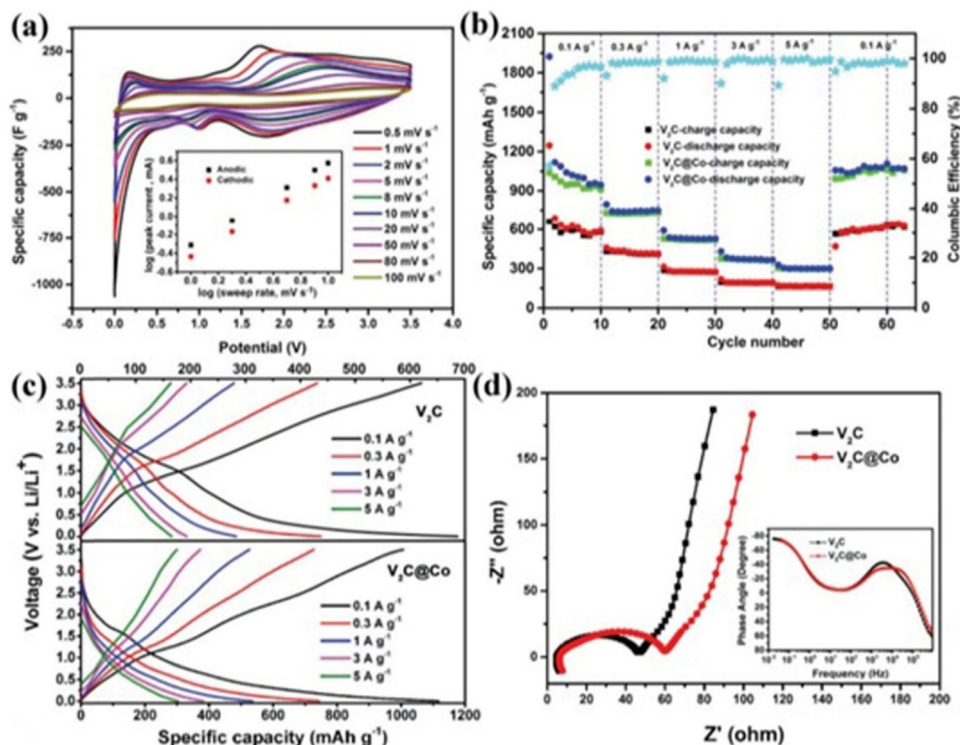
Fig. 5 The performance of the multi-layered V_2C MXene with the intercalation of Co^{2+} ions. (a) Specific capacity curves of the V_2C electrode at different scan rates. Inset: The change in $\log(i)$ vs. $\log(v)$. (b) Rate performance of V_2C and V_2C interlayer engineered electrodes. (c) A comparative analysis of galvanostatic charge and discharge curves under different current densities V_2C and Co^{2+} interlayer-engineered V_2C electrodes. (d) A comparison of the EIS spectra of V_2C and Co^{2+} interlayer-engineered V_2C electrodes. Inset: Impedance phase angle vs. frequency. The images were adapted/reproduced from ref. 142 with permission from Advanced Materials 2018.

cyclability and rate performance.[136] The storage of lithium-ion MXene-based electrodes is greatly influenced by chemical components, surface terminations, doped atoms, and porous structures.[137] Theoretically, it was found that gravimetric capacities vary inversely with the formula weight of the MXenes.[138] It was experimentally shown that Ti_2C exhibited a capacity of 160 mA h g^{-1}, whereas Ti_3C_2 possessed 110 mA h g^{-1} due to the formation of the inactive TiC layer in Ti_3C_2.[139] However, V_2C displayed a higher capacity of 280 mA h g^{-1} than Nb_2C and Ti_2C, indicating the influence of the type of transition metal present, as well as preparation environments.[49] The surfactants like F and OH choke Li$^+$ transportation and inhibit the storage of Li$^+$ in Ti_3C_2 and V_2C, whereas O-functionalized MXenes boost Li$^+$ storage capacity.[140,141] Once we practically formed the pure MXene anodes, we came to know that the reversible capacity was comparatively lower than predicted. A 2D $Hf_3C_2T_z$ MXene was made by introducing silicon to intensify the Al (Si)– C bond and reduce the adhesive energy of the Hf–C bond, exposing a reversible gravimetric capacity of 146 mA h g^{-1} at a current density of 200 mA g^{-1} at the end of 200 cycles.[62]

The introduction of a heteroatom can also alter the properties of MXenes. The intercalation of Co^{2+} ions into multi-layered V_2C MXenes yielded a widened interlayer spacing (9.52 Å) due to the strong V–O–Co bond formation. This method achieved an excellent storage capacity of 1117.3 mA h g^{-1} at 0.1 A g^{-1} and a very long cycling life of

over 15 000 times.[142] The characteristic features of this electrode material for electrochemical storage are shown in Fig. 5. Because there is a reduction in the contents of heteroatoms in the synthesised MXenes, various improvements can be made to make it impressive. Moreover, the improvement of ion diffusion kinetics within the electrode material is also achieved by the pore engineering of MXene-based electrodes. A freestanding MXene 3D macroporous foam was derived from the sulphur-template method to exhibit a high capacity of 455.5 mA h g^{-1} at 50 mA g^{-1}, a high rate capacity of 101 mA h g^{-1} at 18 A g^{-1} and very long cyclic stability.[143] This method can improve the energy density of LIBs, by restricting the usage of Cu/Al current collectors within it.

Another way to improve the existing properties and to hamper the hurdles put forth is by the fabrication of MXene-based hybrids. Compositing 2D MXenes with 0D materials like nanodots, nanospheres and nanoparticles to form LIB electrodes enhances the properties. Herein, the 2D MXene nanosheets remediate the volumetric variance that occurs in charge/discharge cycles and 0D materials restrict the restacking of these layers. This increases the ion diffusion kinetics and storage. The facial CO_2 oxidation of $Nb_4C_3T_x$ and $Ti_3C_2T_x$ gives rise to new 0D hybrids $Nb_2O_5@Nb_4C_3T_x$ and $TiO_2@Ti_3C_2T_x$, respectively. Both composites express higher lithium storage performance when compared to bare MXenes due to the intimate coupling of interfaces.[144] Further strategies have to be invented

to obtain highly coupled interfaces in MXene/0D hybrids for electrodes with better performance. In the sandwich model the 0D materials, MXene layers, and coating layers are assembled, to accommodate their surface pulverization. The fabrication of PVP–Sn(IV)@Ti$_3$C$_2$ sandwiched hybrids can be done by the method of PVP (polyvinyl pyrrolidone)-assisted liquid-phase immersion of Sn nanoparticles into the MXene matrix, delivering an appreciable reversible capacity of 1375 mA h cm^{-2} and high cycling stability after 50 cycles.[145]

The integration of 2D MXenes with 1D nanomaterials like nanofibers, nanowires, nanotubes, nanobelts, nanoribbons, or nanorods, forms MXene/1D hybrids that are either vertically or horizontally loaded. The vertically loaded CNTs and CNFs with MXene nanosheets enhance the overall electrode conductance and rate performance of LIBs.[146,147] Similarly, non-carbon oxides can also be introduced to obtain high transport kinetics and cycling stability with excellent capacity retention.[148] Horizontally loaded TiO$_2$ nanorods and SnO$_2$ nanowires in Ti$_3$C$_2$ not only offer a short lithium diffusion length and additional active sites in the electrode material but also prevent the aggregation of the nanosheets.[149] As a result, a maximum capacity of 138 mA h g^{-1} was achieved at a current density of 2000 mA g^{-1}, claiming its importance in making anode materials for LIBs with excellent power density and energy density.

The horizontal loading of 2D nanomaterials with 2D MXene nanosheets produces improved gravimetric capacity, whereas high-rate anodes with excellent transport kinetics are achieved by vertical loading. The 2D MoS$_2$-on-MXene anode displayed an extraordinary charge capacity of 509 mA h g^{-1} at 0.1 A g^{-1} after 100 cycles, which is much higher than bare Mo$_2$TiC$_2$T$_x$ with a 52 mA h g^{-1} capacity.[150] A facile hydrothermal method was employed in the vertical loading of thin SnO$_x$ nanosheets (~5 nm) uniformly into the layers and surfaces of the Ti$_3$C$_2$ matrix to form SnO$_x$@Ti$_3$C$_2$ composites.[151] They provided an enhanced capacity of 450 mA h g^{-1} at 0.2 A g^{-1} over 250 cycles, revealing the possibilities of further exploring these methods (Table 3).

There are a few other lithium-based batteries, such as lithium–metal batteries, lithium–air batteries and lithium sulphur batteries, which are expected to overrule the area of high-performance batteries.

4.1.1 Lithium–metal batteries. Lithium metal can be conceded as a perfect anode material for lithium-based batteries because of its extremely low potential and high theoretical specific capacity.[165] lithium–metal batteries have attained great popularity in energy storage applications due to their very high theoretical specific capacity of 3860 mA h g^{-1}, very low negative potential (-3.04 V vs. the standard hydrogen electrode), low density of 0.534 g cm^{-3} and the outstanding material flexibility of Li metal. Therefore, they are considered to be the most relevant high-energy density next-generation batteries along with lithium–sulphur batteries, lithium–air batteries and lithium-ion batteries.[86,166] Although this can give rise to lithium batteries with high operating voltage and enhanced energy density, the commercialisation of the Li metal anode is not well appreciated. A serious challenge faced is

Table 3 A brief outlook on the electrochemical performances of MXenes and MXene-based materials for lithium-ion batteries

Electrode material	Current rate (mA g^{-1})	Reversible capacity (mA h g^{-1})	Cycle number	Capacity after cycle (mA h g^{-1})	Ref.
Ti$_2$CT$_x$	0.04C	225	80	110	152
Ti$_3$C$_2$T$_x$	260	123.6	100	118.7	153
Nb$_4$C$_3$	100	310	100	380	154
Sn@V$_2$C	100	1284.6	90	1262.9	155
Ag/Ti$_3$C$_2$	1C	330	5000	310	156
CNTs@Ti$_3$C$_2$	1000	479	250	445	146
Mo$_2$CT$_x$/CNT	5000	560	1000	250	64
Nb$_2$CT$_x$@CNT	2.5C	420	300	430	157
LiMn$_2$O$_4$/Ti$_3$C$_2$T$_x$	1C	—	200	114.1	158
CNF/Ti$_3$C$_2$	1C	320	2900	320S	147
BPQDs/Ti$_3$C$_2$	1000	170	2400	520	159
TiO$_2$(nanorod)/Ti$_3$C$_2$T$_x$	500	204	200	209	149
SnO$_2$(nanowire)/Ti$_3$C$_2$T$_x$	1000	560	500	530	149
Fe$_3$O$_4$@Ti$_3$C$_2$	1C	336.8	1000	747.4	160
Si@SiO$_x$@C/Ti$_3$C$_2$T$_x$	0.2C	1674	200	1547	161
N$_{a0.55}$Mn$_{1.4}$Ti$_{0.6}$O$_4$/Ti$_3$C$_2$T$_x$	5000	440	5000	350.68	162
Bi$_2$MoO$_6$/MXene	100	—	200	692	163
MoS$_2$/Mo$_2$TiC$_2$T$_x$	100	646	100	509	150
(Ti$_3$C$_2$)/rGo	50	335.5	1000	212.5	164
δ-MoN	0.05C	336	200	320	103

dendrite formation on the electrode surface, perforating the diaphragm, which may cause a short circuit and even lead to hazardous situations.[167] Lithium dendrites can be easily peeled off to form "dead lithium" with hindered electrochemical activity, further rapidly diminishing the reversible capacity. However, the large variation in volume, inevitable dendrite formation, short life span low electrode conductivity, and fluctuating solid electrolyte interphase (SEI) films can be named as the major challenges that forestall their commercial applications.[168,169] Therefore, Li metal anodes with large current density (>5 mA cm^{-2}) and high Li loading ($>90\%$), which are dendrite-free, are requisite for high-performance batteries. This can be accomplished by the proper engineering of the metal anodes and by selecting/modifying a suitable electrolyte. Wu et al. devised a dendrite-free Li metal anode by designing a light-weight framework of MXene and graphene.[165] This highly conductive and lithiophilic 3D network enabled the suppression of Li dendrite formation, escalation of storage capacity and compensation of volume changes. Another remarkable feature was the record lifespan of the electrode (2700 h); it showcased stability after 230 cycles at 20 mA cm^{-2}, which is an exceptionally high current density. Zhang et al. developed 3D porous MXene aerogels displaying high electron conductivity, Li$^+$ transport kinetics, and plentiful Li nucleation sites, which act as scaffolds for the Li metal electrode.[168] They ensure the uniform nucleation of the metal ion in the presence of the oxygen-rich surface functionalisation on the MXene sheet. A notable advantage of MXene aerogels is the networked interspaces that help to cushion volume changes and accomplish high lithium loading. Along with all these features, the cross-linked structure of MXene sheets establish a channel for the fast transportation of ions and hence, produced appreciably high cycling stability, even up to a

current density of 10 mA cm^{-2}. In 2019, Yang *et al.* contrived a perpendicular MXene–Li array with tunable MXene walls to achieve a dendrite-free, high-rate electrode material for LMBs.[169] This array was comprised of fixed periodic nanoscale and microscale interspaces, facilitating the fast-paced Li$^+$ transfer while stripping/plating and the homogenization of the electric field, respectively. This electrode resulted a low potential of 25 mV, outstanding capacity of 2056 mA h g^{-1}, and appreciable cycle stability up to 1700 h.

Another way to obtain high-capacity, dendrite-free, long-living electrode materials is by the optimisation of the electrolyte. MXene-based nanocomposite polymer electrolytes (CPEs) can be synthesised for high-performance solid-state LMBs by an aqueous solution blending method.[170] The MXene-based CPEs (MCPEs) fabrication is done by the uniform dispersion of Ti$_3$C$_2$T$_x$ flakes into PEO$_{20}$–LiTFSI (poly (ethylene oxide)/lithium bis(trifluoromethyl sulphonyl)imide) complex. The ionic conductivity of the electrolyte is improved with the introduction of these 2D flakes into PEO, as it encourages segmental motion and obstructs the crystallisation of PEO. It was experimentally derived that CPE with 3.6 wt% MXene exhibited the highest ionic conductivity (2.2×10^{-5} S m^{-1} at 28 °C) at room temperature and the MCPE with 1.5 wt% MXene possessed high-rate capability and stability in comparison to the latest CPELMB. This indicates that MXenes are best compared to other 0D/1D nanofillers, and are armed to enhance the performance of electrolytes for LMBs. Both methods proclaim the significant role played by MXenes in the development and promotion of highly efficient electrode materials for LMBs. Diverse methods of synthesis have resulted in compounds with diverse properties and features. Hence, more methods have to be introduced to make it feasible for the commercialisation of LMBs.

4.1.2 Lithium–sulphur batteries. Lithium–sulphur batteries have attained much attention due to the high capacity, high energy density, simple configuration, and environmentally amiable nature of sulphur materials.[171] Unlike lithium–metal batteries, sulphur is the cathode material of LSBs, which undergoes multi-electron reactions during charging and discharging cycles. However, further applications are restrained for certain reasons. During the charge/discharge cycles, lithium polysulphide intermediates are generated, which rapidly decreases the overall performance of the battery.[172] The dissolution of polysulphide intermediates as well as sulphur in non-aqueous solvents like DMSO, THF, dioxolane and glyme, may lead to its reaction with lithium, which induces the formation of an insulating layer on the surface of the lithium anode, eventually generating severe polarization.[173] Efforts have been made to engineer and select suitable electrode materials to absorb the polysulphides.[174–176] Sulphur is also an insulator that exhibits very low conductivity.[177] Additionally, the conversion of S into Li$_2$S gives rise to a volume expansion of 80% and is not favourable for retaining the electrode stability. MXenes with their extraordinary properties have channelled a new area for the manufacture of

high-capacity Li-based electrode materials. It was also observed that the engineering of MXene nanoribbons effectively improved their electrochemical performance. Dong *et al.* used Ti$_3$C$_2$ nanoribbons as the sulphur host to attain the expected rate performance and durability.[178] The a-Ti$_3$C$_2$-S/d-Ti$_3$C$_2$/PP electrode was prepared by the application of Ti$_3$C$_2$ nanosheets on the polypropylene separator as an interlayer and it hampered the shuttle effect of lithium polysulfide through chemical absorption and physical blocking. This electrode material exhibited a high reversible capacity of 1062 mA h g^{-1} at 0.2C and an enhanced capacity of 632 mA h g^{-1} for up to 50 cycles at 0.5C, which is remarkable when compared with conventional a-Ti$_3$C$_2$-S on an Al current collector. Heteroatom doping can be performed to enhance the cyclic stability and rate capability of LSBs. Bao *et al.* designed N-doped MXene nanosheets by an annealing process, which showed a crumpled morphology as a host material for sulphur.[177] N-Doped MXene nanosheets were experimentally found to have strong physico-chemical adsorption capacities. This facilitates the effective absorption of polysulphides and encourages sulphur loading of 5.1 mg cm^{-2} over a wide area. The crumpled morphology of N-Ti$_3$C$_2$T$_x$/S achieved the expected electrochemical properties with a high reversible capacity of 1144 mA h g^{-1} at 0.2C and the cycling stability was extended to 610 mA h g^{-1} for up to 1000 cycles at 2C. LSBs with the modified Li-metal anode and sulfurized polyacrylonitrile (S@PAN) cathode can produce high capacity and promise a high performance.[179] Also, Mo$_2$CT$_x$ integrated with MXene nanosheets can form S@Mo$_2$CT$_x$, which enhances the ion transport kinetics due to high conductivity and a low diffusion barrier.[180] This material displays a high reversible capacity (918 mA h g^{-1}) at 1C and enhanced cycling stability. Yao *et al.* used first-principles calculations to study S-functionalized Ti$_2$N (Ti$_2$NS$_2$) as the host materials for LSB cathodes and it was found to enhance the conductivity and hinder the shuttle effect.[181] 3D-structured MXene nanosheets can also alleviate the inherent problem of LSBs by absorbing the discharged substances within their porous structure and thereby increasing their conductivity and ion transport.[182,183] The selection of different materials manifested different properties for the synthesised electrode material. A suitable combination of materials/compounds helps in the fabrication of electrode materials with desired properties to make them popular among the manufacturers.

4.1.3 Lithium–air batteries. LABs or lithium–air batteries have acquired great popularity in recent days due to their high energy density (10 times LIBs) and power density and hence they can be employed in future technology for long-range electric vehicles ($>$500 km).[184] The general composition of LABs is a metallic Li anode and a porous cathode (oxygen being the active material) with suitable Li-containing electrolytes that can be aqueous, non-aqueous, hybrid or solid electrolytes.[185] The electrochemical interaction between O$_2$ and Li$^+$ in LABs results in the formation of Li$_2$O$_2$ during the discharge process and is stored within the cathode. Hence, this electrode plays a crucial role in influencing the storage capability of LABs and the reversibility of Li-ions. Even though

Table 4 A summary of the electrochemical performances of MXene-based materials for LABs and LSBs

Electrode material	Current rate (mA g^{-1})	Cycle number	Capacity after cycle (mA h g^{-1})	Rate performance (mA h g^{-1}) at current rate (mA g^{-1})	Ref.
Lithium–sulphur batteries					
MSC-2	167.5(0.1C)	200	946.7	502.3 at 2C	195
Ti$_3$C$_2$T$_x$/S	1675 (1C)	1500	940	1075 at 2C	196
Co-CNT@MXene/S	0.5C	200	600	789.29 at 0.5C	197
a-Ti$_3$C$_2$-S/d-Ti$_3$C$_2$/PP	2C	200	50.4%	288 at 10C	178
S@N-PC/Ti$_3$C$_2$	1C	800	527	595 at 2C	198
Ti$_3$C$_2$T$_x$(4h)-GN	2C	1000	–	663 at 2C	199
S@SA-Zn-MXene	1C	400	706	517 at 2C	200
Ti$_3$C$_2$T$_x$/RGO/S	0.5C	300	878.4	750 at 0.5C	201
S@TiO$_2$/Ti$_2$C	2C	200	464	317.7 at 5C	202
N-Ti$_3$C$_2$T$_x$/S	2C	1000	610	770 at 2C	177
MPP separators	0.5C	500	550	743.7 at 1C	203
CMP separator	1C	600	614	728 at 2C	204
50% S@Ti$_3$C$_2$T$_x$	2C	175	1170	1161 at 2C	205
N-Ti$_3$C$_2$/C@PP separator	0.5C	500	716	675 at 2C	206
79S/CNT-Ti$_3$C$_2$	0.5C	1200	450	510 at 0.5C	172
MX-NF/PP	1C	1000	645	794 at 3C	207
S@V$_2$C–Li/C	0.5C	500	600	400 at 5C	208
T@CP separator	0.25C	200	1100	950 at 2.5C	209
MXene/ESM separator	0.5C	250	877	948 at 1C	210
MXene/1T-2H MoS$_2$-C-S	0.5C	300	799.3	677.2 at 2C	211
Ti$_3$C$_2$T$_x$@AlF$_3$/Ni(OH)$_2$	1C	1000	435	635 at 4C	212
N-RGO/Ti$_3$C$_2$T$_x$	0.5C	200	850	1180 at 0.1C	213
MPF13-550/PP	0.2C	200	721	593 at 2C	214
nMOF-867/Ti$_3$C$_2$T$_x$	1C	1000	801	581 at 4C	215
Graphene/MXene fibre	1C	1000	—	733.3 at 2C	216
S/MXene-CS$_2$/IPA	1C	1000	522.7	1474.5 at 0.1C	217
MXene/CNC/S	0.1C	100	823.8	630.5 at 4C	218
3D S-CNT@MXene	4C	150	656.3	557.3 at 8C	219
Lithium–air batteries					
CoO/Ti$_3$C$_2$T$_x$	100	160	—	8560 at 500	220
V–TiO$_2$/Ti$_3$C$_2$T$_x$	200	100	1000	1.61 V at 800	191
NiO/Ti$_3$C$_2$	500	90	500	5790 at 500	221
LaSrCoO/Ti$_3$C$_2$T$_x$	500	80	1000	1.29 V at 1000	222
Nb$_2$C MXene	3000	130	—	—	223

the lethargic oxygen reduction reaction (ORR) and oxygen evolution reaction (OER) are the critical factors restricting the further development of LABs.[188] It reflects the priority of an efficient catalytic system to improve the reaction rate, thereby enhancing the performance rate and cycle life of LABs. Owing to their large surface area, high electrical conductivity, porous structure and less expensive nature, carbon materials have acquired great popularity in the manufacturing of electrodes in LABs. Irrespective of these advantages, carbon electrodes are generally corrosive and may induce associated reactions and therefore reduce the reaction efficiency of the cathode and the lifetime of the battery.[189] Recent studies revealed that MXenes can emerge as a promising cathode material for LABs due to their structural stability, highly appreciable surface area and outstanding electron/ion conductivity.[190] The combination of a high-yielding catalyst and MXenes can enhance the performance of the electrode materials of LABs. Recently, Zheng *et al.* synthesised a V-TiO$_2$/Ti$_3$C$_2$T$_x$ composite by an ethanol-thermal method that involves the *in situ* growth of high-efficiency catalytic TiO$_2$ nanoparticles with surplus oxygen vacancies on Ti$_3$C$_2$T$_x$ nanosheets.[191] This system possessed certain advantages that encourage its application as a LAB electrode material. TiO$_2$ nanoparticles are tiny and are fixed evenly on multilayer MXene nanosheets, which enhance the stability and make active materials attainable. Another important feature is that MXene can stabilize oxygen vacancies, thus contributing to the improvement of electrons and Li$^+$ transfer kinetics, as they are the active sites for cathodic catalysing reactions. In addition, the multilayer structure of this composite expedites the penetration of the electrolyte and hinders the electrode volume variation caused as a result of the deposition and decomposition of Li$_2$O$_2$. As a result, the V-TiO$_2$/Ti$_3$C$_2$T$_x$ composite when employed as the cathode material displayed a high specific capacity of 11 487 at 100 mA g^{-1}, low overpotential of 0.21 V and appreciable cyclic stability where 93% round-trip efficiency was maintained even after 200 cycles. The dendrite formation hinders the popularisation of LAB. An important way to improve the energy efficiency and block redox shuttling, capacity fading, and electrolyte degradation, is by the use of redox mediators that will decompose the products discharged.[192] Oxygen can lead to the corrosive effects of Li and stabilizing agents like LiNO$_3$ can be used to improve the battery life as it can act as a passivation interface between anodes.[193] The Ti$_2$C MXene with different multifunctional groups can give rise to high-performance LABs with appreciable energy density.[194] However, highly efficient LABs are still under research interest and improvements have to be made to promote them in the market (Table 4).

4.2 MXenes in sodium-ion batteries

Sodium-ion batteries can be viewed as a strong alternative to LIBs with their cost-effectiveness and improved performance rates. However, the large ionic radii of Na$^+$ ions demand electrode materials with large interlayer spacing for their integration. MXenes and their composites that accommodate

they are viewed as the future generation of environmentally amiable rechargeable batteries, their low capacity, low rate capability, large voltage gaps between charging/discharging cycles, and poor cycle life hinder their practical applications.[186,187] Apart from all the problems mentioned,

ions of different sizes can therefore be employed as host materials in SIBs.[136] Along with surface tunability and mechanical flexibility, MXenes can provide a range of working potentials, enabling them to be used as either anodes or cathodes.[224,225] Surface-functionalised MXenes are favourable for the insertion/de-insertion of Na$^+$ ions and show low diffusion lengths. When the Ti$_3$C$_2$T$_x$ MXene is used as the substrate, the resulting anode exhibits appealing rate performance and cyclic stability.[226,227] Later, Yu *et al.* theoretically calculated Na$^+$ storage capacities of 413.0 mA h g^{-1} for interlayer expanded bare Ti$_3$C$_2$, 367.7 mA h g^{-1} for O-terminated Ti$_3$C$_2$, and 151.2 mA h g^{-1} for F-terminated Ti$_3$C$_2$, which occur within negligible volume changes (-0.5% to $+1.6\%$) during intercalation/deintercalation.[228] The doping of heteroatoms is a plausible method for adjusting the structural parameters of MXenes. It was estimated theoretically that a sulphur-doped MXene (Ti$_3$C$_2$S$_2$) exhibited appreciable conductivity and sodium storage capacity and a low diffusion barrier.[229] S-Doped Ti$_3$C$_2$T$_x$, due to their enlarged multilayered morphology and surface-induced capacitance, provided a storage capacity of 183.2 mA h g^{-1} at 100 mA g^{-1} after 100 cycles, an unexpected rate capacity of 113.9 mA h g^{-1} at 4000 mA g^{-1} and outstanding cycling stability for 2000 cycles, surpassing all Ti$_3$C$_2$T$_x$ anodes reported up to that time (<100 mA h g^{-1}).[230] Moreover, with nitrogen being highly electronegative, Ti$_3$CN has emerged as a promising anode material in SIBs, producing a large capacity of 98.9 mA h g^{-1} at 500 mA g^{-1}, which is 1.65 times the capacity of the Ti$_3$C$_2$ anode.[231] Although these results proclaim the improvement in the capacity and rate capability achieved in heteroatom doping, the MXene matrix is comprised of quite low doping contents.

Another way of achieving a high capacity of Na storage, increased rate capacity and ion kinetics is by establishing a pillaring effect, taking the electrostatic interaction of negatively charged MXenes and metal ions into account. Luo *et al.* formed pillared MXene sheets (Na–Ti$_3$C$_2$) with sufficiently enlarged interlayer spacing. The material exhibited an increased reversible capacity of 175 mA h g^{-1} at 0.1 A g^{-1}, which is approximately 170% of the original value, and cycling stability for 2000 cycles at 2.0 A g^{-1}. There was a critical increase in the number of active sites and a decrease in the Na$^+$ diffusion barrier post-Na$^+$ pillaring as compared to that of Ti$_3$C$_2$, Li–Ti$_3$C$_2$, and K–Ti$_3$C$_2$.[232] Even though the nanoengineering of MXene layers has shown a rapid rise in the required properties, the precise tuning of interlayer spaces has not been achieved in all methods.

The introduction of porous structures can also be done to tune the transport properties. The porous Ti$_3$C$_2$T$_x$ electrode possessed capacities of 166 mA h g^{-1} at 1 A g^{-1} and 124 mA h g^{-1} at 10 A g^{-1}. The electrode also delivered a long cycle life of up to 1000 cycles with negligible capacity decay at 1 A g^{-1}.[233] The performance results of these electrodes are displayed in Fig. 6. The enhancement of ion transfer between electrodes can be accomplished by employing PMMA spheres as pore-forming templates. The 2D MXene nanosheets were fully covered by the PMMA spheres and were thermally treated

and filtered in a vacuum to obtain flexible, impressively conductive 3D freestanding porous MXene films. When used as SIB anodes, these films, showed enhanced capacity performances (rate capability and cycling stability).[234]

The fabrication of MXene-based hybrid materials or composites can give rise to high-capacity active materials for high-rated SIBs. An encapsulated TiO$_2$@Ti$_3$C$_2$T$_x$ structure was synthesised by exploiting the electrostatic interactions between MXenes and TiO$_2$ mono-dispersed nanospheres that delivered a reversible capacity of 116 mA h g^{-1} at 960 mA g^{-1} for up to 5000 cycles.[235] Even though metal sulphide anodes possess high specific capacities, bulk materials hinder their cyclability. Therefore, a critical examination has to be done on nanodots with a small diameter (<10 nm) to fully utilise the intrinsic capacity. A composite FeS$_2$@MXene synthesised by the chemical assembly of Ti$_3$C$_2$T$_x$ nanosheets, iron hydroxide, followed by sulphurization resulted in a capacity of 563 mA h g^{-1} at 100 mA g^{-1}.[236] Hence, uniform distribution and the incorporation of sulphides in MXenes enhanced the performance rate of SIB electrodes.

The restacking of MXene nanosheets can be effectively blocked by 1D hybrid materials and can achieve electrodes with high volumetric capacity with the architecture of a horizontally loaded model. MXene/CNTs films were manufactured by electrostatically combining negatively charged Ti$_3$C$_2$ flakes and positively charged CNTs with cetyltrimethyl ammonium bromide modification and then by filtration. This can be directly used as an anode for SIBs and they provide a volumetric capacity of 421 mA h cm^{-3} at 20 mA g^{-1} current density.[237] Similarly, 2D materials can also be loaded horizontally onto MXene nanosheets to get MXene/2D hybrid electrodes. One drawback of this fabrication is that the horizontally loaded model has low ion conductivity. The synthesis of MoS$_2$/Ti$_3$C$_2$T$_x$ composites alleviated this problem and enhanced the ion kinetics in MXene layers by raising the interlayer space and enhancing its specific capacity. When substituted as the anode in SIBs they obtained a specific capacity of 250.9 mA h g^{-1} in 100 cycles along with an extraordinary rate performance of 162.7 mA h g^{-1} at 1 A g^{-1}.[238] However, the poor cyclic stability can be overpowered by engineering a sandwich model to include an outer carbon layer.

4.2.1 Sodium-metal batteries. Another means of sodium storage can be achieved by sodium-metal anodes in sodium-metal batteries (SMBs). Although there is the uncontrollable and uneven formation of dendrites, MXenes have eased their way towards energy storage applications. The host material is to be taken in such a way that it suppresses the metal dendrite formation and optimises the infinite volume expansion and maintains the desired electrochemical performance. Pillared MXenes help in the enhancement of electrochemical performance and rate capability. In addition to the nucleation of Na into the large interlayer space of Sn^{2+}-pillared Ti$_3$C$_2$MXene, the uniform deposition of Na can also be achieved. This pillared SMB electrode yields high current density (up to 10 mA cm^{-2}) and high areal capacity (up to 5 mA h cm^{-2}) for up to 500 cycles. Sodium-metal batteries show higher electrochemical performance.[239]
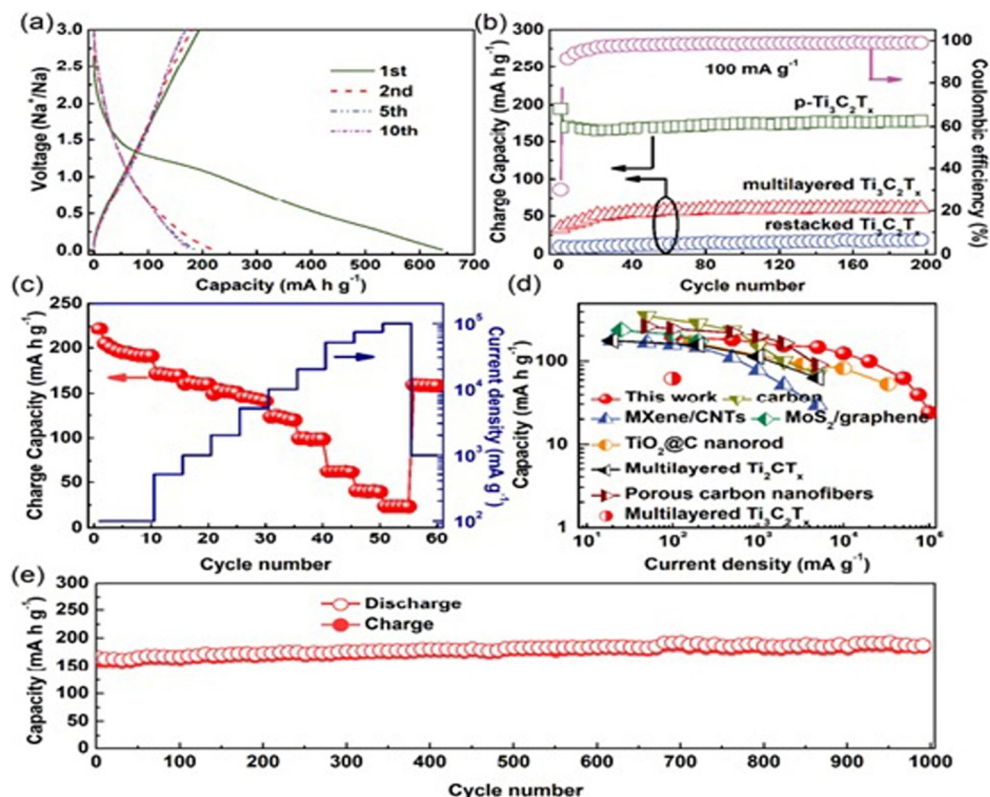
Fig. 6 p-Ti$_3$C$_2$T$_x$ electrodes and half-cell tests: (a) charge/discharge curves of the p-Ti$_3$C$_2$T$_x$ electrodes at 100 mA g^{-1}. (b) Charge capacity and coulombic efficiency vs. the cycle number of the as-prepared p-Ti$_3$C$_2$T$_x$, multi-layered Ti$_3$C$_2$T$_x$, and restacked Ti$_3$C$_2$T$_x$ at 100 mA g^{-1}, as well as the coulombic efficiency vs. cycle number for p-Ti$_3$C$_2$T$_x$. (c) The performance rate of p-Ti$_3$C$_2$T$_x$. (d) A comparative study of the rate capability of p-Ti$_3$C$_2$T$_x$ with some other conventional anode materials. The image was adapted/reproduced from ref. 234 with permission from Advanced Materials 2018.

On reviewing the recent advancements, it was obvious that the electrochemical performance of SIBs is regulated by various factors that include the type of MXenes used, space for intercalation, surface specification, reaction environment and electrode surface properties. Being larger, the diffusion of sodium ions takes more time than Li-ions. Reasonable cycle stability and energy density of SIBs can be achieved by increasing the interlayer spacing, the formation of composites or generating pillared structures. All these strategies can be adopted to improve the electrochemical performance and rate capacity. However, the low capacity and poor rate capability of anodes are still hurdles to the commercial production of SIBs. The architecture of good performance and environmentally friendly MXene-based electrode materials for SIBs opens up a large area for research opportunities.

4.3 MXenes in potassium-ion batteries

PIBs are generally known as the cheapest alkali-ion batteries due to the natural abundance of potassium. Although they possess similar properties to Li and a low potential (-2.93 V), the large ionic radius of potassium (0.138 nm) is the first hurdle to finding a suitable host material for electrodes.[240] The first MXene experimentally found to be suitable to intercalate K$^+$ ions was Ti$_3$CNT$_z$.[241] This resulted in an extraordinary reversible capacity of 75 mA h g^{-1}, after 100 charge–discharge cycles at 20 mA g^{-1}. Interlayer spacing, surface imperfections

and the number of layers can be adjusted to improve the accommodation of K$^+$ ions to obtain electrodes with appreciable cyclic and storage capacity. The SEM micrograph of this Ti$_3$CNT$_z$, specific capacity vs. number of cycles at 20 mA g^{-1} and the structure of Ti$_3$CNO$_2$ before and after electrochemical potassiation and de-potassiation are shown in Fig. 7(a)–(c), respectively.

Ming et al. tried to enhance the K$^+$ storage performance by using the porous K-V$_2$C nanosheets, formed by the subsequent acid/alkali treatment.[242] This brings in a 195 mA h g^{-1} capacity at 50 mA g^{-1}, and better rate performance. Anodes made out of alkalised-Ti$_3$C$_2$ MXene, with its better structure stabilisation, reaction kinetics, 3D porous structure and narrowed networking nanoribbons, delivered a high capacity of 78 mA h g^{-1} at 200 mA g^{-1} while incorporated in PIBs.[243] The capacity can be made even higher with the synthesis of MXene-based derivatives. Dong et al. derived K$_2$Ti$_4$O$_9$ ultrathin nanoribbons by the concurrent oxidation and alkalization of Ti$_3$C$_2$ MXene and obtained a capacity of 151 mA h g^{-1} at 50 mA g^{-1} and 900 times the stable cyclability as compared to normal MXenes.[244] Su et al. synthesised TiO$_2$-RP/CN nanofibers from red phosphorus and TiO$_2$ to obtain a potential anodic material for excellent storage performance for KIBs. In addition to the derivatives, MXene-based hybrids/composites can also increase the capacity and rate performance of electrode materials. A vertically aligned sandwich model of carbon-coated MoSe$_2$/
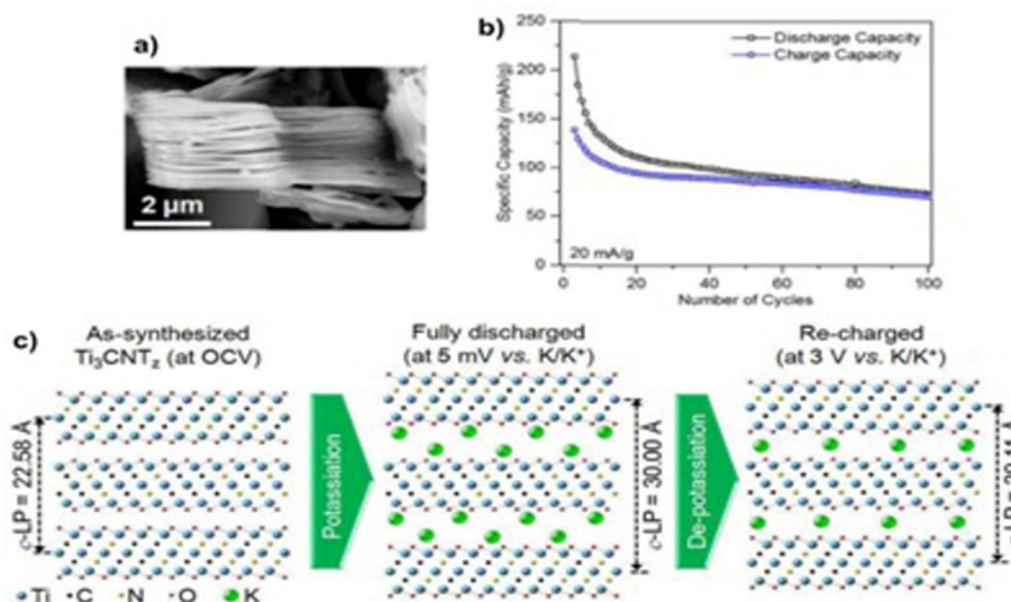
Fig. 7 (a) SEM Micrograph of Ti_3CNT_z. (b) Specific capacity *vs.* number of cycles at 20 mA g^{-1}. (c) Schematic representation of Ti_3CNO_2 before and after electrochemical potassiation and de-potassiation. The image was adapted/reproduced from ref. 241 with permission from Chemical Communications 2017.

MXene hybrid nanosheets exhibited high conductivity and durability as a superior electrode material for PIBs.[75] The vertical alignment prevented the severe stacking of MXene nanosheets, improved its structural stability, and the reinforcement of the composite structure by the carbon layer enhanced its electronic conductivity. As a result, MoSe$_2$/MXene@C acquired a reversible capacity of 355 mA h g^{-1} at 200 mA g^{-1} and magnificent rate performance of 183 mA h g^{-1} at 10.0 mA g^{-1}, even after 100 cycles, making it the most advantageous electrode material for PIBs as compared to the conventional MXenes. Another method of producing high-density PIBs is by using MXene/K hybrid anodes. A defect-rich MXene ($Ti_{3-x}CNT_y$) established the freestanding scaffold as a metal K host that controls nucleation to make it free of dendrites.[246] These DN MXenes in the scaffold are generally potassium-philic, thereby encouraging the K nucleation during cycling, which strictly prevents the direct plating of K outside of the scaffold to obtain a dendrite-free morphology, high coulombic efficiency of 98.6% and a long cycle life up to 300 h. They can also be employed in potassium-sulphur anodes to get better performance. A very recent finding in 2021 was the formation of microorganism-derived MXene@N-doped CNF(carbon nanofibre) anode materials that provided high-performance PIBs.[247] In this method of bio-adsorption, *Aspergillus niger* biofungal nanoribbons were the substrate and $Ti_3C_2T_x$ nanosheets were assembled on them to obtain a 2D/1D heterostructure. This MXene-based N-doped CNF structure with sufficient fully opened pores, eases the ion kinetics and gives a high reversible capacity and stability.

4.4 MXenes in magnesium-ion batteries

MIBs have drawn considerable research attention due to their benign and hazardless nature, despite several challenges. Their low cost and abundant sources also inflate the curiosity for further explorations to employ them in large-scale renewable energy storage applications. The divalent nature of Mg^{2+} ions comes with a reduction in transport kinetics that eventually dampens the reversible capacity and output power of the electrodes.[248] Research strategies implemented to develop required cathode materials initially ended in polyanions, chalcogenides and Chevrel phase cathodes. However more suitable materials have to be investigated to ensure high capacity and stability during the charge/discharge cycles and rate performance. MXenes were theoretically found to be suitable for the manufacturing of the electrodes for MIBs, as they can ensure stable multilayer intercalation.[32] Djire *et al.* found that nanolayered Ti_2NT_x, with a high multilayer adsorption rate for Mg^{2+} ions on Ti_2NT_x nanosheets, exhibited exemplary reversible redox peaks and a wide working voltage.[249] By the end of 1000 cycles, they successfully reproduced a capacitance of 200 F g^{-1} at 500 mA g^{-1} that increased up to 160% of its initial value, when placed in a safe and hazardless Mg-ion electrolyte. The introduction of Mg^{2+} ions from a magnesium electrolyte into the 3D microporous $Ti_3C_2T_x$ MXene sheets was done to increase the reversible capacity and to test the performance of MIB cathodes.[250] The $Mg_{0.21}Ti_3C_2T_x$ cathode displayed plausible cycling stabilities of 210 mA h g^{-1} at 0.5C, 140 mA h g^{-1} at 1C, 55 mA h g^{-1} at 5C and appreciable rate performance. The large irreversible capacity explained by the redox reaction mechanism should be kept increasing to prevent capacity decay. MXene-based nanocomposites can also increase the durability and storage capacity of the electrodes. Another method used for making cathodes with high-rate performance and cyclability is the electrostatic incorporation of negatively charged MXene nanosheets and space-consuming positively charged carbonaceous nanospheres. Liu *et al.* successfully

synthesized the $Ti_3C_2T_x$@C cathode to achieve a notable reversible specific capacity of 198.7 mA h g^{-1} at 10 mA g^{-1} and rate capacity of 123.3 mA h g^{-1} at 200 mA g^{-1}.[251] These hybrid materials are characterised by improved cyclic stability with 85% capacity retention after 400 cycles. This method of synthesis forbids MXene layer restacking and widens the interlayer spacing to foster ion-transport kinetics and permeation of the electrolyte. Similarly, a durable V_2CT_x@C hybrid was also derived by this method and found to have a storage capacity of 75.4 mA h g^{-1} at 10 mA g^{-1}. Xu *et al.* vertically loaded MoS_2 between $Ti_3C_2T_x$ nanosheets, using a single-step hydrothermal method to obtain a petal-like MoS_2/MXene composite.[252] Even though this hybrid gives an appreciable reversible capacity of 165 mA h g^{-1} at 50 mA g^{-1} and high rate performance of 93 mA h g^{-1} at 200 mA g^{-1}, it cannot be considered for commercialisation. A very recent study devised the synthesis of the PI@$Ti_3C_2T_x$ composite through electrostatic self-assembly

within a mild reaction environment that hindered the oxide formation of $Ti_3C_2T_x$.[253] The 3D composite showed a high tapped density ($\sim$1.12 g cm^{-3}), amplified electrical conductivity ($\sim$3.26 $\times$ 10^{-2} S cm^{-1}), supreme storage of aqueous Mg^{2+}, eminent rate capability and durability. All these methods open up the possibility for further research for forming commercially viable and exploitable electrode materials for MIBs.

4.5 MXenes in calcium-ion batteries

Calcium is the fifth most abundant element in nature. With their attractive reduction potential (-2.87 *vs.* NHE) and reduced polarizability, the ions are expected to have high reaction speed and power output.[254] However, suitable host materials are required for the fast integration and de-insertion of Ca^{2+} ions. MXene nanosheets, owing to their high conductivity, surface functionalisation and intercalation volume, serve as a substantial host for manufacturing cathodes for CIBs.

Table 5 A brief outlook on the superior electrochemical performances of MXenes and MXene-based materials for non-lithium batteries

Electrode material	Current rate (mA g^{-1})	Cycle number	Capacity after cycle (mA h g^{-1})	Rate performance (mA h g^{-1}) at current rate (mA g^{-1})	Ref.
Sodium-ion batteries					
Ti_3C_2/NiCoP	1000	2000	261.7	416.9 at 100	255
a-Ti_3C_2	200	500	50	168 at 20	243
c-$Ti_3C_2T_x$	20	50	246	120 at 500	256
p-$Ti_3C_2T_x$	1000	1000	189	166 at 1000	233
f-$Ti_3C_2T_x$_DMSO	1000	1500	76	110 at 2000	257
2D MXene/SnS_2	100	125	120	78 at 2000	258
VO_2/MXene	100	200	280.9	206 at 1600	259
Sulphur-decorated Ti_3C_2	2000	1000	135	136.6 at 5000	260
3D V_2CT_x	500	1000	310	170 at 5000	234
PDDA-BP/Ti_3C_2	100	2000	658	461 at 2000	261
Sb_2O_3/$Ti_3C_2T_x$	100	100	472	295 at 2000	262
Bi_2S_3/MXene	500	250	155	168 at 5000	263
$NaTi_{1.5}O_{8.3}$	200	150	130	101 at 2000	244
Ti_3CN	500	500	60	98.8 at 500	231
$MoSe_2$/MXene	2000	400	384	250 at 10 000	264
$NiCoS_4$@ReS_2	1000	500	396	297 at 3000	265
rGO/p-$Ti_3C_2T_x$	1000	1000	84.8%	280 at 100	266
ZnSe@NCNF	10 000	1700	197.3	–	267
$CoSe_2$@CNT	2000	200	400	280 at 2000	268
$Ti_3C_2T_x$/graphene	2500	100	220	600 at 50	269
$Na_{0.23}TiO_2$/Ti_3C_2	2000	4000	56	178 at 5000	270
Ti_3C_2-Sb_2S_3	200	300	475	410 at 1000	271
Potassium-ion batteries					
M-KTO, $K_2Ti_4O_9$	50	900	151	88 at 300	244
a-Ti_3C_2	200	500	42	60 at 300	243
$MoSe_2$/MXene@C	100	300	317	183 at 10 000	245
PDDA-NPCN/Ti_3C_2	1000	2000	252.2	254.8 at 1000	272
MXene/MoS_2	200	50	145.5	168.2 at 500	273
(MoS_2/N, P-rGO)	2000	7000	236.6	224.9 at 20 000	274
$Ti_3C_2T_x$@Sb	500	500	79.1435	270 at 500	275
SnS_2 NSs/MXene	500	200	206.1	342.4 at 50	276
$Fe_{x-1}Se_x$/MXene/FCR	100	80	449.3	15.3 at 1000	277
MXene-bonded HC	50	100	210	102.2 at 500	278
BPE@V_2CT_x	2000	3000	261	229.6 at 2000	279
NG/$ReSe_2$/MXene	5000	300	90	137.5 at 10 000	280
MXene@NCNF	1000	1000	201.5	—	247
Magnesium-ion batteries					
$Ti_3C_2T_x$@C	50	400	140.6	123.3 at 200	251
3D $Mg_{0.21}Ti_3C_2T_x$	100	60	50	55 at 500	250
MnO_2/MXene–Ti_3C_2	50	100	105	21 at 500	281
$Ti_3C_2T_x$/CTAB	200	250	135	32 at 2000	282
MoS_2/MXene	50	50	108	93 at 200	252
d-$Ti_3C_2T_x$/CNT(Hybrid Mg^{2+}/Li$^+$ batteries)					283

Table 6 A summary of the electrochemical performances of MXene-based materials for alkali metal batteries

Electrode material	Cyclic performance	Rate performance	Ref.
Lithium–metal batteries			
PA-MXene-Li	Lifespan of 900 cycles at 1 mA cm^{-2}	$\sim$0.4 V at 15 mA cm^{-2}	284
MXene-MF-Li	Lifespan of 3800 h at 10 mA cm^{-2}	$\sim$0.085 V at 50 mA cm^{-2}	285
MXene@CNF/Li	Lifespan over 1300 h at 0.5 mA cm^{-2}	—	286
Zn/MXene films	Lifespan of 1200 h at 1 mA cm^{-2} and capacity 1 mA h cm^{-2}	0.14 V at 8 mA cm^{-2}	287
MXene@NPSi@C	Lifespan over 800 cycles at 2 mA cm^{-2}	—	288
MXene–Li arrays	2500 cycles at 20 mA cm^{-2}	-25 mV at 20 mA cm^{-2}	169
Ti$_3$C$_2$/rGO scaffolds	350 cycles at 10 mA cm^{-2} and capacity 1 mA h cm^{-2}	42 mV at 10 mA cm^{-2}	168
3DP-MXene arrays-Li	Lifespan of 1200 h at 1.0 mA cm^{-2}	$\sim$100 mV at 20 mA cm^{-2}	289
Laser-MXene-50	1500 h (750 cycles) at 1 mA cm^{-2}	—	290
MXene/liquid-metal film	Lifespan over 350 h at 0.5 mA cm^{-2}	78.4 mV at 1.2 mA cm^{-2}	291
3D MXene/graphene	230 cycles at 20 mA cm^{-2}	$\sim$13 mV at 3 mA cm^{-2}	165
Ti$_3$C$_2$T$_x$@Zn@Li	Stable over 600 cycles at 1 mA cm^{-2}	—	292
C/TiO$_2$@Li‖LiFePO$_4$	Stable over 250 cycles at 1C	59 mA h g^{-1} even at 3.0C	293
Li TiO$_2$-Li$_3$N-C	Lifespan of 2000 h at 1 mA cm^{-2}	30 mV at 1 mA cm^{-2}	294
MXene/AgNW scaffold	3000 h lifespan at 20 mA cm^{-2}	—	295
Sodium metal batteries			
h-Ti$_3$C$_2$T$_x$/CNT	Lifespan over 4000 h at 1.0 mA cm^{-2} and capacity 1.0 mA h cm^{-2}	46 mV at 5 mA cm^{-2}	296
Na-Ti$_3$C$_2$T$_x$-CC	Lifespan over 300 h at 3 mA cm^{-2} and capacity 1.0 mA h cm^{-2}	$\sim$0.35 V at 9 mA cm^{-2}	297
CT-Sn(II)@Ti$_3$C$_2$	Lifespan over 500 cycles at 4 mA cm^{-2}	40 mV at 4 mA cm^{-2}	239
C-NTO-3/Na	Lifespan over 400 cycles at 3 mA cm^{-2} and capacity 3 mA h cm^{-2}	—	298
MXene-MF-Na	720 h at 10 mA cm^{-2}	$\sim$15 mV at 20 mA cm^{-2}	285
Potassium metal batteries			
MXene-MF-K	800 h at 5 mA cm^{-2}	—	285
K@DN-MXene/CNT	300 h at 0.5 mA cm^{-2}	0.40 V at 2 mA cm^{-2}	246
a-Ti$_3$C$_2$	700 h at 10 mA cm^{-2}	—	299
K-ACM	230 h at 1 mA cm^{-2}	$\approx$0.31 V at 5 mA cm^{-2}	300

Xie *et al.* predicted that MXene nanosheets functionalised with O can easily incorporate Ca^{2+} ions within the layers.[32] Through theoretical simulation, it was found that Ti$_2$CO$_2$ has a notable storage capacity of 487 mA h g^{-1} for Ca^{2+}, as compared to the monovalent Na$^+$ and K$^+$ ions, with capacities of 288 and 264 mA h g^{-1}, respectively. Since the smallest Ca^{2+} ions show negligible interactions with each other on intercalation with Ti$_3$C$_2$, more ions can be adsorbed and a storage capacity of 319.8 mA h g^{-1} is gained. This indicates that the adsorption energy decreases as there is an increase in the number of ions adsorbed.[31] Meanwhile, the integration of Ca^{2+} ions in Ti$_2$CO$_2$/graphene and V$_2$CO$_2$/graphene heterostructures produced reliable storage capability and stability. However, the theoretical predictions and simulations are meaningless if the electrodes are not practically synthesised. Considering the manufacturing techniques of LIBs, SIBs, MIBs and PIBs, further studies can be done to discover a feasible, stable and efficient electrode material for CIBs. Porous nanomaterials can also be attributed to these applications as they can accommodate large-sized ions (Tables 5–7).

5. Conclusions

This review has mainly focused on the recent innovations made in the field of energy storage using MXenes and MXene-based composites in various alkali-ion batteries, including LIBs, SIBs, PIBs, MIBs and CIBs. On evaluating heteroatom integration, the loaded model, encapsulated model, sandwiched model and cost-effective metal host electrodes, we encountered great potential and good performances of MXenes and their hybrids,

making them efficient and suitable for energy storage. We also observed that MXenes can be substituted as conductive substrates, and even current collectors in various MIBs, which could increase the density of the electrode material and the maximum usage of the material. In spite of these advantages, MXene-based electrodes still face limitations that prevent their application in large-scale production. All these controlling factors are to be evaluated for further exploration.

(1) Synthesis methods and reaction environments can affect the expected electrochemical performance and yield of the electrodes made out of MXenes and their derivatives, along with the type of transition material used, interlayer spacing, and surface functional groups (O, OH, F, *etc.*). It was also observed that the surface/bulk morphology of the nanosheets greatly affected the rate and storage capacity of the electrodes. Certain surface functional groups can either enhance or hinder the electrode performance. Since F and Cl terminations decrease the rate capacity of metal-ion batteries, synthetic methods have to be adopted in such a way that it prevents the functionalisation with these elements. However currently used top-down methods retain these elements within them. In addition, the HF-involved etching methods are considered to be environmentally hazardous. Interestingly, Lewis acid etching and bottom-up methods like chemical vapour deposition (CVD) may promote the achievement of high-purity MXenes devoid of these surfactants. The decline in the yield, number of layers and high synthesis cost limit the large-scale application of CVD. Further research can be conducted to make it economically feasible and efficient, as pure MXenes can be employed as current collectors in metal-ion batteries, superconductors and separation processes.

Table 7 A comparative study on the advantages and disadvantages of using MXene in various alkaline batteries

Type of battery	Advantages	Ref.	Disadvantages	Ref.
Lithium-ion batteries	• Being flexible, they stay as a conductive scaffold as well as a multifunctional binder for other materials.	44	• MXenes are highly expensive and denser	
	• Build strong connectivity within the composites.	301	• Misinterpretation of the performance data	
	• Continuous variation in the oxidation state of transition metals can boost specific capacity.	302	• MXenes are oxidised quickly, thus limiting commercialisation.	44
	• Consistent and rapid lithium storage			
Lithium–sulphur batteries	• Entrap the long-chain and short-chain poly-sulphides with suitable termination.	133	• If MXene is used in excess (>10% of total sulphur), it lowers the energy density	
	• Suppression of the shuttle phenomenon	303	• A dark inert condition for both storage and operation is compulsorily maintained to retain the inherent properties of MXenes.	304
	• Enhances the charge storage capacity as well as the life cycle.			
	• Improved utilization of the sulphur due to rapid charge transfer ability.			
Lithium-air batteries	• Improved overall rate performance.	190	• Although DFT studies have been reported for LABs, only a small number of MXenes candidates are being exploited.	305
	• Enable to sketch the way of Li_2O_2 formation.			
	• Enhance the rate of ion/electron migration.			
Lithium–metal batteries	• Mitigate dendrite formation.	306	• Aggregation of MXene intersheets during plating as well as stripping of Li metal diminishes the lithiophilic interfaces and intercalation space.	307
	• Compensate volume changes		• The brittle nature of 3 D MXenes cannot tolerate the strain generated by Li plating, thereby it reduces stability as well as reversibility	
	• Increased lifespan of the electrode.			
	• Li metal can be nucleated and grown uniformly	286		
Sodium-ion batteries	• Lower diffusion activation energy is established	308	• MXene matrix offers lower doping contents.	231
	• Enhances transport kinetics and performance rate	309	• De-sodiation capability is lower for pure MXene than other alloying materials	310
	• Uniform distribution is ensured by their increased surface area.	233	• Pure MXenes produce low reversible capacity	309
	• Porous MXenes improve transport characteristics.			
Sodium–metal batteries	• MXene composites prevent the formation of dead Na	19	• The direct inclination of Na onto the MXene matrix surface may give rise to dendrite formation sites.	239
	• The pillar effect can enhance the accommodation of more Na	239		
Potassium-ion batteries	• Enhanced electric conductivity		• Poor potassium storage capability	
	• Lower K^+ diffusion barrier	308	• Expeditious capacity degradation	308
Magnesium-ion batteries	• Increase durability and storage capacity.	250	• The occurrence of a positive charge on the MXene surface causes repulsion with Mg^{2+} ions that eventually affects desolvation.	
	• Enhance electrolytic permeability.	251	• Fluorine and hydroxyl terminations affect average voltages.	311

(2) The use of nanospheres, porous/pillared structures and doping of heteroatoms can also increase the capacity and rate even after many charge/discharge cycles. The heteroatom introduction provides excellent storage capacity and ion diffusion kinetics in LIBs and SIBs, as it increases the interlayer spacing significantly. The compositing of 2D MXene nanosheets with 0D/1D/2D nanomaterials forms hybrids that redeem the volumetric variance that occurs in charge/discharge cycles and restrict the MXene layer restacking to enhance the increase in the ion diffusion kinetics and storage. The porous MXenes, when tested in SIBs, exhibited dominant capacity, rate capability and stability in comparison with the non-pillared materials, and reserved 98.5% capacity within the 50th and 100th cycles. This promises the requirement of pillaring techniques applied to MXenes, providing a new approach to optimizing their properties for a range of applications, including energy storage, conversion, catalysis, and gas separations. Even though MXenes were initially introduced for making electrode materials, eventually, their modification helped them to prevent dendrite formation, form substrates for intercalation, block the MXene restacking, provide active sites and encourage diffusion kinetics.

(3) On considering the rechargeable non-Li-ion batteries, we came to realise that even though theoretical predictions have offered a bright hope for SIB application, experimental results proposed low capacity and poor rate capability for the existing anodes synthesised to date. Initial studies advocated that the introduction of carbon materials like CNTs could develop freestanding electrodes, though low reversible capacity remained an obstacle for future developments. Even though multivalent ion batteries like MIBs are an appealing alternative due to their abundance, low dendrite electrodes, and high volumetric

energy capacity, their low operation voltage and high ion-migration barrier restrain further applications.

(4) Other Li-based batteries like LSBs, LMBs and LABs were able to modify the electrochemical performance, energy density and capacity in comparison with the prevailing LIBs. A magnificent incident happened in the design of a 3D conductive $Ti_3C_2T_x$ MXene–melamine foam (MXene–MF) by Shi et al., which turned out to be a universal host material for Na, K and Li.[285] Their works substantiated the effectiveness of MXenes in hindering the growth of metal dendrites within the electrode material. However, ideal anode/cathode materials that can be exploited as commercial electrodes for Li-based batteries are still residing in the green room.

(5) Lastly, the applications of MXene-based electrodes should be analysed with supreme importance. MXenes can be employed as conductive additives, 2D conductive substrates in electrode materials that possess high capacity, and as a protective layer on metal anodes in various MIBs. The MXene-based fibres can find applications in electrically operated vehicles. Moreover, they are incorporated in fibre-based batteries to increase conductivity, flexibility and lower the internal resistance to obtain highly efficient and cost-effective batteries. Since these fibres can be moulded and framed into different shapes and sizes, they can be used in wearable electronics and flexible devices.

Recently, a lot of bio-derived MXenes and MXene-based hybrids have attained high popularity since they possess appreciable capacity and stability. The nanoengineering of various microstructures such as 3D hybrids and sandwich-like structures should be done to produce favourable specific surface area, pore sizes, and pore size distribution. The nanostructures synthesised artificially have great potential for solving some pivotal issues that may occur during cycling, thereby enhancing the reversible capacity and cycle life of the batteries. However, the manufacture of high-capacity MXene-based nanostructures/nanocomposites with high retention capacity is still in the dormant stage. Increased research in this field can only enhance their properties to ensure their further practical applications. The hydrophilicity of MXene layers can also be studied in depth to incorporate that feature in AIBs to achieve versatile properties. Theoretical predictions made in the case of divalent alkali-ion batteries should be discovered in the coming years. In looking forward, MXene-based nanomaterials can be used to make smart AIBs that may possess various properties, opening the gateway towards the manufacture of next-generation batteries, electrochemical energy vehicles and wearable devices.

Author contributions

Helen Treasa Mathew: Conceptualization, investigation, writing-original draft preparation, writing-review and editing. Kumar Abhisek: writing-review and editing, visualization. Shashikant Shivaji Vhatkar: writing-review and editing, visualization.
Ramesh Oraon: funding acquisition, resources, supervision, validation, writing-review and editing.

Conflicts of interest

The authors declare no conflict of interest.

Acknowledgements

References

1 Y. Y. Deng, K. Blok and K. van der Leun, Transition to a fully sustainable global energy system, Energy Strateg. Rev., 2012, 1(2), 109–121, DOI: 10.1016/J.ESR.2012.07.003.

2 N. S. Lewis, Toward Cost-Effective Solar Energy Use, Science, 2007, 315(5813), 798–801, DOI: 10.1126/SCIENCE.1137014.

3 W. Li, et al., Rational Design and General Synthesis of Multimetallic Metal–Organic Framework Nano-Octahedra for Enhanced Li–S Battery, Adv. Mater., 2021, 33(45), 2105163, DOI: 10.1002/ADMA.202105163.

4 F. Jamil, H. M. Ali and M. M. Janjua, MXene based advanced materials for thermal energy storage: a recent review, J. Energy Storage, 2021, 35, 102322, DOI: 10.1016/J.EST.2021.102322.

5 D. P. Van Vuuren, et al., Stabilizing greenhouse gas concentrations at low levels: an assessment of reduction strategies and costs, Clim. Chang., 2007, 81(2), 119–159, DOI: 10.1007/S10584-006-9172-9.

6 X. Wu, Y. Ru, Y. Bai, G. Zhang, Y. Shi and H. Pang, PBA composites and their derivatives in energy and environmental applications, Coord. Chem. Rev., 2022, 451, 214260, DOI: 10.1016/J.CCR.2021.214260.

7 X. Zheng, et al., Multifunctional RGO/Ti3C2Tx MXene fabrics for electrochemical energy storage, electromagnetic interference shielding, electrothermal and human motion detection, Mater. Des., 2021, 200, 109442, DOI: 10.1016/J.MATDES.2020.109442.

8 Y. Jiang, F. Guo, Y. Liu, Z. Xu and C. Gao, Three-dimensional printing of graphene-based materials for energy storage and conversion, SusMat, 2021, 1(3), 304–323, DOI: 10.1002/SUS2.27.

9 A. S. Aricò, P. Bruce, B. Scrosati and J. M. Tarascon, and W. Van Schalkwijk, Nanostructured materials for advanced energy conversion and storage devices, Mater. Sustain. Energy A Collect. Peer-Reviewed Res. Rev. Artic. from Nat. Publ. Gr, 2010, 148–159, DOI: 10.1142/9789814317665_0022.

10 Z. D. Hao, X. Xu, H. Wang, J. Liu and H. Yan, Research Progress on Surface Coating Layers on the Positive

Electrode for Lithium Ion Batteries, *Nano*, 2018, **13**(11), 1–15, DOI: **10.1142/S1793292018300074**.

11 Y. Wu, Y. Sun, J. Zheng, J. Rong, H. Li and L. Niu, Exploring MXene-based materials for next-generation rechargeable batteries, *J. Phys. Energy*, 2021, **3**(3), 032009, DOI: **10.1088/2515-7655/abf14d**.

12 R. Petri, T. Giebel, B. Zhang, J. H. Schünemann and C. Herrmann, Material cost model for innovative li-ion battery cells in electric vehicle applications, *Int. J. Precis. Eng. Manuf. Technol.*, 2015, **2**(3), 263–268, DOI: **10.1007/S40684-015-0031-X**.

13 W. Zhang, H. Jin, G. Chen and J. Zhang, Sandwich-like N-doped carbon nanotube@Nb2C MXene composite for high performance alkali ion batteries, *Ceram. Int.*, 2021, **47**(14), 20610–20616, DOI: **10.1016/j.ceramint.2021.04.070**.

14 J. Y. Hwang, S. T. Myung and Y. K. Sun, Sodium-ion batteries: present and future, *Chem. Soc. Rev.*, 2017, **46**(12), 3529–3614, DOI: **10.1039/c6cs00776g**.

15 J. Muldoon, C. B. Bucur and T. Gregory, Quest for Non-aqueous Multivalent Secondary Batteries: Magnesium and Beyond, *Chem. Rev.*, 2014, **114**(23), 11683–11720, DOI: **10.1021/CR500049Y**.

16 E. G. Ahn, J. H. Yang and J. H. Lee, $Mg_3Si_3(MoO_6)_2$ as a High-Performance Cathode Active Material for Magnesium-Ion Batteries, *ACS Appl. Mater. Interfaces*, 2021, **13**(40), 47749–47755, DOI: **10.1021/acsami.1c16896**.

17 X. B. Cheng, *et al.*, Dendrite-Free Lithium Deposition Induced by Uniformly Distributed Lithium Ions for Efficient Lithium Metal Batteries, *Adv. Mater.*, 2016, **28**(15), 2888–2895, DOI: **10.1002/adma.201506124**.

18 W. Zhang, W. K. Pang, V. Sencadas and Z. Guo, Understanding High-Energy-Density Sn4P3 Anodes for Potassium-Ion Batteries, *Joule*, 2018, **2**(8), 1534–1547, DOI: **10.1016/j.joule.2018.04.022**.

19 Y. Dong, H. Shi and Z. S. Wu, Recent Advances and Promise of MXene-Based Nanostructures for High-Performance Metal Ion Batteries, *Adv. Funct. Mater.*, 2020, **30**(47), 1–24, DOI: **10.1002/adfm.202000706**.

20 Y. Dong, Z. S. Wu, W. Ren, H. M. Cheng and X. Bao, Graphene: a promising 2D material for electrochemical energy storage, *Sci. Bull.*, 2017, **62**(10), 724–740, DOI: **10.1016/j.scib.2017.04.010**.

21 M. Naguib, V. N. Mochalin, M. W. Barsoum and Y. Gogotsi, 25th Anniversary Article: MXenes: A New Family of Two-Dimensional Materials, *Adv. Mater.*, 2014, **26**(7), 992–1005, DOI: **10.1002/ADMA.201304138**.

22 M. W. Barsoum, *MAX phases: Properties of machinable ternary carbides and nitrides*, Wiley-VCH, 2013, DOI: **10.1002/9783527654581**.

23 V. H. Nowotny, Strukturchemie einiger Verbindungen der Übergangsmetalle mit den elementen C, Si, Ge, Sn, *Prog. Solid State Chem.*, 1971, **5**(C), 27–70, DOI: **10.1016/0079-6786(71)90016-1**.

24 L. Verger, C. Xu, V. Natu, H. M. Cheng, W. Ren and M. W. Barsoum, Overview of the synthesis of MXenes and other ultrathin 2D transition metal carbides and

nitrides, *Curr. Opin. Solid State Mater. Sci.*, 2019, **23**(3), 149–163, DOI: **10.1016/j.cossms.2019.02.001**.

25 B. Anasori, J. Halim, J. Lu, C. A. Voigt, L. Hultman and M. W. Barsoum, Mo_2TiAlC_2: a new ordered layered ternary carbide, *Scr. Mater.*, 2015, **101**, 5–7, DOI: **10.1016/j.scriptamat.2014.12.024**.

26 Z. Liu, L. Zheng, L. Sun, Y. Qian, J. Wang and M. Li, $(Cr_{2/3}Ti_{1/3})_3AlC_2$ and $(Cr_{5/8}Ti_{3/8})_4AlC_3$: New MAX-phase Compounds in Ti–Cr–Al–C System, *J. Am. Ceram. Soc.*, 2014, **97**(1), 67–69, DOI: **10.1111/JACE.12731**.

27 Q. Tao, *et al.*, Two-dimensional Mo1.33C MXene with divacancy ordering prepared from parent 3D laminate with in-plane chemical ordering, *Nat. Commun.*, 2017, **8**(1), 1–7, DOI: **10.1038/ncomms14949**.

28 M. Anayee, *et al.*, Role of acid mixtures etching on the surface chemistry and sodium ion storage in $Ti_3C_2T_x$M-Xene, *Chem. Commun.*, 2020, **56**(45), 6090–6093, DOI: **10.1039/d0cc01042a**.

29 Y. Sun, D. Chen and Z. Liang, Two-dimensional MXenes for energy storage and conversion applications, *Mater. Today Energy*, 2017, **5**, 22–36, DOI: **10.1016/J.MTENER.2017.04.008**.

30 D. Wang, Y. Lin, D. Hu, P. Jiang and X. Huang, Multifunctional 3D-MXene/PDMS nanocomposites for electrical, thermal and triboelectric applications, *Composites, Part A*, 2020, **130**, 105754, DOI: **10.1016/J.COMPOSITESA.2019.105754**.

31 D. Er, J. Li, M. Naguib, Y. Gogotsi and V. B. Shenoy, Ti_3C_2 MXene as a High Capacity Electrode Material for Metal (Li, Na, K, Ca) Ion Batteries, *ACS Appl. Mater. Interfaces*, 2014, **6**(14), 11173–11179, DOI: **10.1021/AM501144Q**.

32 Y. Xie, *et al.*, Prediction and Characterization of MXene Nanosheet Anodes for Non-Lithium-Ion Batteries, *ACS Nano*, 2014, **8**(9), 9606–9615, DOI: **10.1021/NN503921J**.

33 K. Fan, Y. Ying, X. Li, X. Luo and H. Huang, Theoretical Investigation of V_3C_2 MXene as Prospective High-Capacity Anode Material for Metal-Ion (Li, Na, K, and Ca) Batteries, *J. Phys. Chem. C*, 2019, **123**(30), 18207–18214, DOI: **10.1021/ACS.JPCC.9B03963**.

34 A. Sinha, *et al.*, MXene: an emerging material for sensing and biosensing, *TrAC, Trends Anal. Chem*, 2018, **105**, 424–435, DOI: **10.1016/J.TRAC.2018.05.021**.

35 M. Xin, J. Li, Z. Ma, L. Pan and Y. Shi, MXenes and Their Applications in Wearable Sensors, *Front. Chem.*, 2020, **8**, 297, DOI: **10.3389/fchem.2020.00297**.

36 J. Wang, Y. Yang and Y. Xia, Mesoporous MXene/ZnO nanorod hybrids of high surface area for UV-activated NO_2 gas sensing in ppb-level, *Sens. Actuators, B*, 2022, **353**, 131087, DOI: **10.1016/J.SNB.2021.131087**.

37 J. Peng, X. Chen, W. J. Ong, X. Zhao and N. Li, Surface and Heterointerface Engineering of 2D MXenes and Their Nanocomposites: Insights into Electro- and Photocatalysis, *Chem*, 2019, **5**(1), 18–50, DOI: **10.1016/J.CHEMPR.2018.08.037**.

38 H. Liu, *et al.*, Structural evolution of MXenes and their composites for electromagnetic interference shielding applications, *Nanoscale*, 2022, **14**(26), 9218–9247, DOI: **10.1039/D2NR02224A**.

39 G. Gao, S. Yang, S. Wang and L. Li, Construction of 3D porous MXene supercapacitor electrode through a dual-step freezing strategy, *Scr. Mater.*, 2022, **213**, 114605, DOI: **10.1016/J.SCRIPTAMAT.2022.114605**.

40 P. Kuang, J. Low, B. Cheng, J. Yu and J. Fan, MXene-based photocatalysts, *J. Mater. Sci. Technol.*, 2020, **56**, 18–44, DOI: **10.1016/j.jmst.2020.02.037**.

41 Y. Vasseghian, E. N. Dragoi, F. Almomani and V. T. Le, A comprehensive review on MXenes as new nanomaterials for degradation of hazardous pollutants: deployment as heterogeneous sonocatalysis, *Chemosphere*, 2022, **287**, 132387, DOI: **10.1016/j.chemosphere.2021.132387**.

42 S. Ganesan, K. R. Ethiraj, M. K. Kesarla and A. Palaniappan, Biomedical Applications of MXenes, *Eng. Mater.*, 2022, 271–300, DOI: **10.1007/978-3-031-05006-0_11**.

43 Y. J. Zhang, *et al.*, Adsorption of uranyl species on hydroxylated titanium carbide nanosheet: a first-principles study, *J. Hazard. Mater.*, 2016, **308**, 402–410, DOI: **10.1016/J.JHAZMAT.2016.01.053**.

44 M. Greaves, S. Barg and M. A. Bissett, MXene-Based Anodes for Metal-Ion Batteries, *Batter. Supercaps*, 2020, **3**(3), 214–235, DOI: **10.1002/BATT.201900165**.

45 M. Li, *et al.*, Halogenated Ti_3C_2MXenes with Electrochemically Active Terminals for High-Performance Zinc Ion Batteries, *ACS Nano*, 2021, **15**(1), 1077–1085, DOI: **10.1021/acsnano.0c07972**.

46 J. Nan, *et al.*, Nanoengineering of 2D MXene-Based Materials for Energy Storage Applications, *Small*, 2021, **17**(9), 1–20, DOI: **10.1002/smll.201902085**.

47 K. Zhu, *et al.*, Synthesis of Ti_2CT_x MXene as electrode materials for symmetric supercapacitor with capable volumetric capacitance, *J. Energy Chem*, 2019, **31**, 11–18, DOI: **10.1016/J.JECHEM.2018.03.010**.

48 A. Vahidmohammadi, A. Hadjikhani, S. Shahbazmohamadi and M. Beidaghi, Two-Dimensional Vanadium Carbide (MXene) as a High-Capacity Cathode Material for Rechargeable Aluminum Batteries, *ACS Nano*, 2017, **11**(11), 11135–11144, DOI: **10.1021/acsnano.7b05350**.

49 M. Naguib, *et al.*, New Two-Dimensional Niobium and Vanadium Carbides as Promising Materials for Li-Ion Batteries, *J. Am. Chem. Soc.*, 2013, **135**(43), 15966–15969, DOI: **10.1021/JA405735D**.

50 B. Soundiraraju and B. K. George, Two-Dimensional Titanium Nitride (Ti_2N) MXene: Synthesis, Characterization, and Potential Application as Surface-Enhanced Raman Scattering Substrate, *ACS Nano*, 2017, **11**(9), 8892–8900, DOI: **10.1021/ACSNANO.7B03129**.

51 R. Meshkian, L. Å. Näslund, J. Halim, J. Lu, M. W. Barsoum and J. Rosen, Synthesis of two-dimensional molybdenum carbide, Mo2C, from the gallium based atomic laminate Mo2Ga2C, *Scr. Mater*, 2015, **108**, 147–150, DOI: **10.1016/J.SCRIPTAMAT.2015.07.003**.

52 M. Naguib, *et al.*, Two-Dimensional Transition Metal Carbides, *ACS Nano*, 2012, **6**(2), 1322–1331, DOI: **10.1021/NN204153H**.

53 M. Naguib, *et al.*, Two-Dimensional Nanocrystals Produced by Exfoliation of Ti_3AlC_2, *Adv. Mater.*, 2011, **23**(37), 4248–4253, DOI: **10.1002/ADMA.201102306**.

54 P. A. Rasheed, R. P. Pandey, T. Gomez, M. Naguib and K. A. Mahmoud, Large interlayer spacing Nb_4C_3T:X(MXene) promotes the ultrasensitive electrochemical detection of Pb^{2+} on glassy carbon electrodes, *RSC Adv.*, 2020, **10**(41), 24697–24704, DOI: **10.1039/d0ra04377j**.

55 M. H. Tran, *et al.*, Adding a New Member to the MXene Family: Synthesis, Structure, and Electrocatalytic Activity for the Hydrogen Evolution Reaction of $V_4C_3T_x$, *ACS Appl. Energy Mater.*, 2018, **1**(8), 3908–3914, DOI: **10.1021/ACSAEM.8B00652**.

56 B. Anasori, *et al.*, Two-Dimensional, Ordered, Double Transition Metals Carbides (MXenes), *ACS Nano*, 2015, **9**(10), 9507–9516, DOI: **10.1021/ACSNANO.5B03591**.

57 B. Anasori, *et al.*, Two-Dimensional, Ordered, Double Transition Metals Carbides (MXenes, *ACS Nano*, 2015, **9**(10), 9507–9516, DOI: **10.1021/acsnano.5b03591**.

58 Q. Tao, *et al.*, Two-dimensional $Mo_{1.33}C$ MXene with divacancy ordering prepared from parent 3D laminate with in-plane chemical ordering, *Nat. Commun.*, 2017, **8**(1), 14949, DOI: **10.1038/NCOMMS14949**.

59 J. Halim, *et al.*, Synthesis of two-dimensional nb1.33c (mxene) with randomly distributed vacancies by etching of the quaternary solid solution $(Nb_{2/3}Sc_{1/3})_2AlC$ max phase, *ACS Appl. Nano Mater.*, 2018, **1**(6), 2455–2460, DOI: **10.1021/acsanm.8b00332**.

60 B. Anasori, *et al.*, A Tungsten-Based Nanolaminated Ternary Carbide: $(W,Ti)_4C_{4−x}$, *Inorg. Chem.*, 2019, **58**(2), 1100–1106, DOI: **10.1021/acs.inorgchem.8b02226**.

61 J. Zhou, *et al.*, A Two-Dimensional Zirconium Carbide by Selective Etching of Al_3C_3 from Nanolaminated $Zr_3Al_3C_5$, *Angew. Chem., Int. Ed.*, 2016, **55**(16), 5008–5013, DOI: **10.1002/ANIE.201510432**.

62 J. Zhou, *et al.*, Synthesis and Electrochemical Properties of Two-Dimensional Hafnium Carbide, *ACS Nano*, 2017, **11**(4), 3841–3850, DOI: **10.1021/ACSNANO.7B00030**.

63 S. Kajiyama, *et al.*, Sodium-Ion Intercalation Mechanism in MXene Nanosheets, *ACS Nano*, 2016, **10**(3), 3334–3341, DOI: **10.1021/acsnano.5b06958**.

64 J. Halim, *et al.*, Synthesis and Characterization of 2D Molybdenum Carbide (MXene), *Adv. Funct. Mater.*, 2016, **26**(18), 3118–3127, DOI: **10.1002/ADFM.201505328**.

65 F. Liu, *et al.*, Preparation of High-Purity V_2C MXene and Electrochemical Properties as Li-Ion Batteries, *J. Electrochem. Soc.*, 2017, **164**(4), A709–A713, DOI: **10.1149/2.0641704JES**.

66 M. Ghidiu, M. R. Lukatskaya, M. Q. Zhao, Y. Gogotsi and M. W. Barsoum, Conductive two-dimensional titanium carbide 'clay' with high volumetric capacitance, *Nature*, 2014, **516**(7529), 78–81, DOI: **10.1038/NATURE13970**.

67 C. (John) Zhang, Interfacial assembly of two-dimensional MXenes, *J. Energy Chem.*, 2021, **60**, 417–434, DOI: **10.1016/J.JECHEM.2020.12.036**.

68 P. Collini, S. Kota, A. D. Dillon, M. W. Barsoum and A. T. Fafarman, Electrophoretic Deposition of Two-Dimensional Titanium Carbide (MXene) Thick Films, *J. Electrochem. Soc.*, 2017, **164**(9), D573–D580, DOI: **10.1149/2.0211709JES/XML**.

69 J. Halim, *et al.*, Transparent Conductive Two-Dimensional Titanium Carbide Epitaxial Thin Films, *Chem. Mater.*, 2014, **26**(7), 2374–2381, DOI: **10.1021/CM500641A**.

70 C. Shen, *et al.*, Synthesis and Electrochemical Properties of Two-Dimensional RGO/$Ti_3C_2T_x$ Nanocomposites, *Nanomaterials*, 2018, **8**, 2, DOI: **10.3390/NANO8020080**.

71 P. Urbankowski, *et al.*, Synthesis of two-dimensional titanium nitride Ti_4N_3 (MXene), *Nanoscale*, 2016, **8**(22), 11385–11391, DOI: **10.1039/C6NR02253G**.

72 K. Maleski and M. Alhabeb, Top-Down MXene Synthesis (Selective Etching), *2D Met. Carbides Nitrides Struct. Prop. Appl.*, 2019, 69–87, DOI: **10.1007/978-3-030-19026-2_5**.

73 M. Naguib, *et al.*, On the Topotactic Transformation of Ti_2AlC into a Ti–C–O–F Cubic Phase by Heating in Molten Lithium Fluoride in Air, DOI: **10.1111/j.1551-2916.2011.04896.x**.

74 M. Ghidiu, J. Halim, S. Kota, D. Bish, Y. Gogotsi and M. W. Barsoum, Ion-Exchange and Cation Solvation Reactions in Ti_3C_2 MXene, *Chem. Mater.*, 2016, **28**(10), 3507–3514, DOI: **10.1021/ACS.CHEMMATER.6B01275**.

75 M. Ghidiu, *et al.*, Alkylammonium Cation Intercalation into Ti_3C_2 (MXene): Effects on Properties and Ion-Exchange Capacity Estimation, *Chem. Mater.*, 2017, **29**(3), 1099–1106, DOI: **10.1021/ACS.CHEMMATER.6B04234**.

76 G. Lv, J. Wang, Z. Shi and L. Fan, Intercalation and delamination of two-dimensional MXene ($Ti_3C_2T_x$) and application in sodium-ion batteries, *Mater. Lett.*, 2018, **219**, 45–50, DOI: **10.1016/J.MATLET.2018.02.016**.

77 V. Natu, M. Sokol, L. Verger and M. W. Barsoum, Effect of Edge Charges on Stability and Aggregation of $Ti_3C_2T_z$ MXene Colloidal Suspensions, *J. Phys. Chem. C*, 2018, **122**(48), 27745–27753, DOI: **10.1021/ACS.JPCC.8B08860**.

78 Y. Omomo, T. Sasaki, L. Wang and M. Watanabe, Redoxable Nanosheet Crystallites of MnO_2 Derived via Delamination of a Layered Manganese Oxide, *J. Am. Chem. Soc.*, 2003, **125**(12), 3568–3575, DOI: **10.1021/JA021364P**.

79 L. Verger, C. Xu, V. Natu, H. M. Cheng, W. Ren and M. W. Barsoum, Overview of the synthesis of MXenes and other ultrathin 2D transition metal carbides and nitrides, *Curr. Opin. Solid State Mater. Sci.*, 2019, **23**(3), 149–163, DOI: **10.1016/j.cossms.2019.02.001**.

80 Y. Z. Zhang, *et al.*, MXene hydrogels: fundamentals and applications, *Chem. Soc. Rev.*, 2020, **49**(20), 7229–7251, DOI: **10.1039/D0CS00022A**.

81 M. Naguib, *et al.*, Two-dimensional transition metal carbides, *ACS Nano*, 2012, **6**(2), 1322–1331, DOI: **10.1021/NN204153H**.

82 X. Fu, *et al.*, Controlled Assembly of MXene Nanosheets as an Electrode and Active Layer for High-Performance Electronic Skin, *Adv. Funct. Mater.*, 2021, **31**(17), 1–8, DOI: **10.1002/adfm.202010533**.

83 J. Tang, *et al.*, Interlayer Space Engineering of MXenes for Electrochemical Energy Storage Applications, *Chem. – Eur. J.*, 2021, **27**(6), 1921–1940, DOI: **10.1002/chem.202002283**.

84 Y. Gogotsi and B. Anasori, The Rise of MXenes, *ACS Nano*, 2019, **13**(8), 8491–8494, DOI: **10.1021/ACSNANO.9B06394**.

85 J. Yang, *et al.*, Two-Dimensional Nb-Based M_4C_3 Solid Solutions (MXenes), *J. Am. Ceram. Soc.*, 2016, **99**(2), 660–666, DOI: **10.1111/JACE.13922**.

86 X. Tang, X. Guo, W. Wu and G. Wang, 2D Metal Carbides and Nitrides (MXenes) as High-Performance Electrode Materials for Lithium-Based Batteries, *Adv. Energy Mater.*, 2018, **8**(33), 1801897, DOI: **10.1002/AENM.201801897**.

87 X. Zhang, Z. Zhang and Z. Zhou, MXene-based materials for electrochemical energy storage, *J. Energy Chem.*, 2018, **27**(1), 73, DOI: **10.1016/J.JECHEM.2017.08.004**.

88 P. Simon, Two-Dimensional MXene with Controlled Interlayer Spacing for Electrochemical Energy Storage, *ACS Nano*, 2017, **11**(3), 2393–2396, DOI: **10.1021/ACSNANO.7B01108**.

89 J. Liu, *et al.*, Hydrophobic, Flexible, and Lightweight MXene Foams for High-Performance Electromagnetic-Interference Shielding, *Adv. Mater.*, 2017, **29**, 38, DOI: **10.1002/ADMA.201702367**.

90 B. Anasori, M. R. Lukatskaya and Y. Gogotsi, 2D metal carbides and nitrides (MXenes) for energy storage, *Nat. Rev. Mater.*, 2017, **2**(2), 1–17, DOI: **10.1038/natrevmats.2016.98**.

91 Y. Bai, *et al.*, MXene-Copper/Cobalt Hybrids via Lewis Acidic Molten Salts Etching for High Performance Symmetric Supercapacitors, *Angew. Chemie*, 2021, **133**(48), 25522–25526, DOI: **10.1002/ANGE.202112381**.

92 X. Li, *et al.*, In Situ Electrochemical Synthesis of MXenes without Acid/Alkali Usage in/for an Aqueous Zinc Ion Battery, *Adv. Energy Mater.*, 2020, **10**(36), 2001791, DOI: **10.1002/AENM.202001791**.

93 T. Li, *et al.*, Fluorine-Free Synthesis of High-Purity $Ti_3C_2T_x$ (T = OH, O) via Alkali Treatment, *Angew. Chem., Int. Ed.*, 2018, **57**(21), 6115–6119, DOI: **10.1002/ANIE.201800887**.

94 Y. Li, *et al.*, A general Lewis acidic etching route for preparing MXenes with enhanced electrochemical performance in non-aqueous electrolyte, *Nat. Mater.*, 2020, **19**(8), 894–899, DOI: **10.1038/S41563-020-0657-0**.

95 V. Kamysbayev, *et al.*, Covalent surface modifications and superconductivity of two-dimensional metal carbide MXenes, *Science*, 2020, **369**(6506), 979–983, DOI: **10.1126/SCIENCE.ABA8311**.

96 Y. Dall'Agnese, M. R. Lukatskaya, K. M. Cook, P. L. Taberna, Y. Gogotsi and P. Simon, High capacitance of surface-modified 2D titanium carbide in acidic electrolyte, *Electrochem. commun.*, 2014, **48**, 118–122, DOI: **10.1016/J.ELECOM.2014.09.002**.

97 W. Sun, *et al.*, Electrochemical etching of Ti_2AlC to Ti_2CT_x (MXene) in low-concentration hydrochloric acid solution, *J. Mater. Chem. A*, 2017, **5**(41), 21663–21668, DOI: **10.1039/C7TA05574A**.

98 Z. Sun, *et al.*, Selective Lithiation–Expansion–Microexplosion Synthesis of Two-Dimensional Fluoride-Free Mxene, *ACS Mater. Lett.*, 2019, **1**(6), 628–632, DOI: **10.1021/ACSMATERIALSLETT.9B00390**.

99 Y. Gogotsi, Chemical vapour deposition: transition metal carbides go 2D, *Nat. Mater.*, 2015, **14**(11), 1079–1080, DOI: **10.1038/NMAT4386**.

100 C. Xu, *et al.*, Large-area high-quality 2D ultrathin Mo2C superconducting crystals, *Nat. Mater.*, 2015, **14**(11), 1135–1141, DOI: **10.1038/NMAT4374**.

101 Y. Fan, L. Huang, D. Geng and W. Hu, Controlled growth of Mo_2C pyramids on liquid Cu surface, *J. Semicond.*, 2020, **41**(8), 082001, DOI: **10.1088/1674-4926/41/8/082001**.

102 Z. Wang, *et al.*, Metal Immiscibility Route to Synthesis of Ultrathin Carbides, Borides, and Nitrides, *Adv. Mater.*, 2017, **29**(29), 1700364, DOI: **10.1002/ADMA.201700364**.

103 S. Joshi, Q. Wang, A. Puntambekar and V. Chakrapani, Facile Synthesis of Large Area Two-Dimensional Layers of Transition-Metal Nitride and Their Use as Insertion Electrodes, *ACS Energy Lett.*, 2017, **2**(6), 1257–1262, DOI: **10.1021/ACSENERGYLETT.7B00240**.

104 F. Zhang, *et al.*, Plasma-enhanced pulsed-laser deposition of single-crystalline Mo_2C ultrathin superconducting films, *Phys. Rev. Mater*, 2017, **1**(3), 034002, DOI: **10.1103/PHYSREVMATERIALS.1.034002**.

105 U. U. Rahman, *et al.*, MXenes as Emerging Materials: Synthesis, Properties, and Applications, *Molecules*, 2022, **27**(15), 4909, DOI: **10.3390/molecules27154909**.

106 S. Sun, C. Liao, A. M. Hafez, H. Zhu and S. Wu, Two-dimensional MXenes for energy storage, *Chem. Eng. J.*, 2018, **338**(2017), 27–45, DOI: **10.1016/j.cej.2017.12.155**.

107 L. MR, *et al.*, Cation intercalation and high volumetric capacitance of two-dimensional titanium carbide, *Science*, 2013, **341**(6153), 1502–1505, DOI: **10.1126/SCIENCE.1241488**.

108 A. Miranda, J. Halim, M. W. Barsoum and A. Lorke, Electronic properties of freestanding $Ti_3C_2T_x$ MXene monolayers, *Appl. Phys. Lett.*, 2016, **108**(3), 033102, DOI: **10.1063/1.4939971**.

109 B. Aïssa, A. Ali, K. A. Mahmoud, T. Haddad and M. Nedil, Transport properties of a highly conductive 2D $Ti_3C_2T_x$ MXene/graphene composite, *Appl. Phys. Lett.*, 2016, **109**(4), 1–6, DOI: **10.1063/1.4960155**.

110 Y. Ando and S. Watanabe, First-principles study of metal-insulator control by ion adsorption on Ti_2C MXene dioxide monolayers, *Appl. Phys. Express*, 2016, **9**(1), 015001, DOI: **10.7567/APEX.9.015001**.

111 K. Hantanasirisakul, *et al.*, Fabrication of $Ti_3C_2T_x$ MXene Transparent Thin Films with Tunable Optoelectronic Properties, *Adv. Electron. Mater*, 2016, **2**(6), 1–7, DOI: **10.1002/aelm.201600050**.

112 M. Kurtoglu, M. Naguib, Y. Gogotsi and M. W. Barsoum, First principles study of two-dimensional early transition metal carbides, *MRS Commun.*, 2012, **2**(4), 133–137, DOI: **10.1557/MRC.2012.25**.

113 V. N. Borysiuk, V. N. Mochalin and Y. Gogotsi, Molecular dynamic study of the mechanical properties of two-dimensional titanium carbides $Ti_{n+1}C_n$ (MXenes), *Nanotechnology*, 2015, **26**(26), 265705, DOI: **10.1088/0957-4484/26/26/265705**.

114 Y. Bai, K. Zhou, N. Srikanth, J. H. L. Pang, X. He and R. Wang, Dependence of elastic and optical properties on surface terminated groups in two-dimensional MXene monolayers: a first-principles study, *RSC Adv.*, 2016, **6**(42), 35731–35739, DOI: **10.1039/C6RA03090D**.

115 Z. Guo, J. Zhou, C. Si and Z. Sun, Flexible two-dimensional $Ti_{n+1}C_n$ ($n = 1$, 2 and 3) and their functionalized MXenes predicted by density functional theories, *Phys. Chem. Chem. Phys.*, 2015, **17**(23), 15348–15354, DOI: **10.1039/C5CP00775E**.

116 J.-C. Lei, X. Zhang and Z. Zhou, Recent advances in MXene: preparation, properties, and applications, *Front. Phys.*, 2015, **10**(3), 276–286, DOI: **10.1007/S11467-015-0493-X**.

117 M. Naguib, *et al.*, $Ti_3C_2T_x$ (MXene)–polyacrylamide nanocomposite films, *RSC Adv.*, 2016, **6**(76), 72069–72073, DOI: **10.1039/C6RA10384G**.

118 Q. Yang, *et al.*, Recent Progress of MXene-Based Nanomaterials in Flexible Energy Storage and Electronic Devices, *Energy Environ. Mater.*, 2018, **1**(4), 183–195, DOI: **10.1002/eem2.12023**.

119 M. Seredych, *et al.*, High-Temperature Behavior and Surface Chemistry of Carbide MXenes Studied by Thermal Analysis, *Chem. Mater.*, 2019, **31**(9), 3324–3332, DOI: **10.1021/ACS.CHEMMATER.9B00397**.

120 I. Ihsanullah, Potential of MXenes in Water Desalination: Current Status and Perspectives, *Nano-Micro Lett.*, 2020, **12**(1), 1–20, DOI: **10.1007/S40820-020-0411-9**.

121 Z. Zheng, *et al.*, The oxidation and thermal stability of two-dimensional transition metal carbides and/or carbonitrides (MXenes) and the improvement based on their surface state, *Inorg. Chem. Front.*, 2021, **8**(9), 2164–2182, DOI: **10.1039/D1QI00041A**.

122 V. Natu, J. L. Hart, M. Sokol, H. Chiang, M. L. Taheri and M. W. Barsoum, Edge Capping of 2D-MXene Sheets with Polyanionic Salts To Mitigate Oxidation in Aqueous Colloidal Suspensions, *Angew. Chem., Int. Ed*, 2019, **58**(36), 12655–12660, DOI: **10.1002/ANIE.201906138**.

123 Y. Zheng, W. Chen, Y. Sun, C. Huang, Z. Wang and D. Zhou, High conductivity and stability of polystyrene/MXene composites with orientation-3D network binary structure, *J. Colloid Interface Sci*, 2021, **595**, 151–158, DOI: **10.1016/J.JCIS.2021.03.095**.

124 C. Wu, C. Huang, Z. Zhang, Y. Xie, Z. Gao and H. Wang, Bulk $Ti_3C_2T_x$ anodes for superior sodium storage performance: the unique role of O-termination, *Mater. Chem. Front.*, 2021, **5**(6), 2810–2823, DOI: **10.1039/D0QM01073A**.

125 I. Persson, *et al.*, On the organization and thermal behavior of functional groups on Ti_3C_2 MXene surfaces in vacuum, *2D Mater*, 2018, **5**(1), 015002, DOI: **10.1088/2053-1583/aa89cd**.

126 M. Ashton, K. Mathew, R. G. Hennig and S. B. Sinnott, Predicted Surface Composition and Thermodynamic Stability of MXenes in Solution, *J. Phys. Chem. C*, 2016, **120**(6), 3550–3556, DOI: **10.1021/ACS.JPCC.5B11887**.

127 B. Anasori, *et al.*, Control of electronic properties of 2D carbides (MXenes) by manipulating their transition metal layers, *Nanoscale Horiz.*, 2016, **1**(3), 227–234, DOI: **10.1039/C5NH00125K**.

128 F. Shahzad, *et al.*, Electromagnetic interference shielding with 2D transition metal carbides (MXenes), *Science*, 2016, **353**(6304), 1137–1140, DOI: **10.1126/SCIENCE.AAG2421**.

129 Y. Liu, H. Xiao, I. William and A. Goddard, Schottky-Barrier-Free Contacts with Two-Dimensional Semiconductors by

Surface-Engineered MXenes, *J. Am. Chem. Soc.*, 2016, **138**(49), 15853–15856, DOI: **10.1021/JACS.6B10834**.

130 M. Khazaei, M. Arai, T. Sasaki, A. Ranjbar, Y. Liang and S. Yunoki, OH-terminated two-dimensional transition metal carbides and nitrides as ultralow work function materials, *Phys. Rev. B: Condens. Matter Mater. Phys.*, 2015, **92**(7), 075411, DOI: **10.1103/PhysRevB.92.075411**.

131 S. Zhao, W. Kang and J. Xue, Manipulation of electronic and magnetic properties of M2C (M = Hf, Nb, Sc, Ta, Ti, V, Zr) monolayer by applying mechanical strains, *Appl. Phys. Lett.*, 2014, **104**(13), 133106, DOI: **10.1063/1.4870515**.

132 J. Hu, B. Xu, C. Ouyang, S. A. Yang and Y. Yao, Investigations on V2C and V2CX2 (X = F, OH) Monolayer as a Promising Anode Material for Li Ion Batteries from First-Principles Calculations, *J. Phys. Chem. C*, 2014, **118**(42), 24274–24281, DOI: **10.1021/JP507336X**.

133 F. Ming, H. Liang, G. Huang, Z. Bayhan and H. N. Alshareef, MXenes for Rechargeable Batteries Beyond the Lithium-Ion, *Adv. Mater.*, 2021, **33**(1), 2004039, DOI: **10.1002/ADMA.202004039**.

134 X. Guo, *et al.*, Ultrasmall metal (Fe, Co, Ni) nanoparticles strengthen silicon oxide embedded nitrogen-doped carbon superstructures for long-cycle-life Li-ion-battery anodes, *Chem. Eng. J.*, 2022, **432**, 134413, DOI: **10.1016/J.CEJ.2021.134413**.

135 D. Di Lecce, R. Verrelli and J. Hassoun, Lithium-ion batteries for sustainable energy storage: recent advances towards new cell configurations, *Green Chem*, 2017, **19**(15), 3442–3467, DOI: **10.1039/C7GC01328K**.

136 J. Pang, *et al.*, Applications of 2D MXenes in energy conversion and storage systems, *Chem. Soc. Rev.*, 2019, **48**(1), 72–133, DOI: **10.1039/C8CS00324F**.

137 L. Xue, S. V. Savilov, V. V. Lunin and H. Xia, Self-Standing Porous LiCoO2 Nanosheet Arrays as 3D Cathodes for Flexible Li-Ion Batteries, *Adv. Funct. Mater.*, 2018, **28**(7), 1705836, DOI: **10.1002/ADFM.201705836**.

138 C. Eames and M. S. Islam, Ion Intercalation into Two-Dimensional Transition-Metal Carbides: Global Screening for New High-Capacity Battery Materials, *J. Am. Chem. Soc.*, 2014, **136**(46), 16270–16276, DOI: **10.1021/JA508154E**.

139 O. Mashtalir, *et al.*, Intercalation and delamination of layered carbides and carbonitrides, *Nat. Commun.*, 2013, **4**(1), 1716, DOI: **10.1038/NCOMMS2664**.

140 Y. Xie, *et al.*, Role of surface structure on Li-ion energy storage capacity of two-dimensional transition-metal carbides, *J. Am. Chem. Soc.*, 2014, **136**(17), 6385–6394, DOI: **10.1021/JA501520B**.

141 Q. Tang, Z. Zhou and P. Shen, Are MXenes Promising Anode Materials for Li Ion Batteries? Computational Studies on Electronic Properties and Li Storage Capability of Ti3C2 and Ti3C2X2 (X = F, OH) Monolayer, *J. Am. Chem. Soc.*, 2012, **134**(40), 16909–16916, DOI: **10.1021/JA308463R**.

142 C. Wang, *et al.*, Atomic Cobalt Covalently Engineered Interlayers for Superior Lithium-Ion Storage, *Adv. Mater.*, 2018, **30**, 32, DOI: **10.1002/ADMA.201802525**.

143 Q. Zhao, *et al.*, Flexible 3D Porous MXene Foam for High-Performance Lithium-Ion Batteries, *Small*, 2019, **15**, 51, DOI: **10.1002/SMLL.201904293**.

144 C. (John) Zhang, *et al.*, Layered Orthorhombic Nb2O5@Nb4C3Tx and TiO2@Ti3C2Tx Hierarchical Composites for High Performance Li-ion Batteries, *Adv. Funct. Mater.*, 2016, **26**(23), 4143–4151, DOI: **10.1002/ADFM.201600682**.

145 J. Luo, *et al.*, Sn4+ Ion Decorated Highly Conductive Ti3C2 MXene: Promising Lithium-Ion Anodes with Enhanced Volumetric Capacity and Cyclic Performance, *ACS Nano*, 2016, **10**(2), 2491–2499, DOI: **10.1021/ACSNANO.5B07333**.

146 W. Zheng, P. Zhang, J. Chen, W. B. Tian, Y. M. Zhang and Z. M. Sun, In situ synthesis of CNTs@Ti3C2 hybrid structures by microwave irradiation for high-performance anodes in lithium ion batteries, *J. Mater. Chem. A*, 2018, **6**(8), 3543–3551, DOI: **10.1039/C7TA10394H**.

147 Z. Lin, D. Sun, Q. Huang, J. Yang, M. W. Barsoum and X. Yan, Carbon nanofiber bridged two-dimensional titanium carbide as a superior anode for lithium-ion batteries, *J. Mater. Chem. A*, 2015, **3**(27), 14096–14100, DOI: **10.1039/C5TA01855B**.

148 J. Sui, X. Chen, Y. Li, W. Peng, F. Zhang and X. Fan, MXene derivatives: synthesis and applications in energy convention and storage, *RSC Adv.*, 2021, **11**(26), 16065–16082, DOI: **10.1039/D0RA10018H**.

149 Y. T. Liu, *et al.*, Self-Assembly of Transition Metal Oxide Nanostructures on MXene Nanosheets for Fast and Stable Lithium Storage, *Adv. Mater.*, 2018, **30**(23), 1707334, DOI: **10.1002/ADMA.201707334**.

150 C. Chen, *et al.*, MoS2-on-MXene Heterostructures as Highly Reversible Anode Materials for Lithium-Ion Batteries, *Angew. Chem., Int. Ed.*, 2018, **57**(7), 1846–1850, DOI: **10.1002/ANIE.201710616**.

151 X. Sun, Y. Liu, J. Zhang, L. Hou, J. Sun and C. Yuan, Facile construction of ultrathin SnOx nanosheets decorated MXene (Ti3C2) nanocomposite towards Li-ion batteries as high performance anode materials, *Electrochim. Acta*, 2019, **295**, 237–245, DOI: **10.1016/J.ELECTACTA.2018.10.152**.

152 L. Huang, T. Li, Q. Liu and J. Gu, Fluorine-free Ti3C2Tx as anode materials for Li-ion batteries, *Electrochem. Commun.*, 2019, **104**, 106472, DOI: **10.1016/J.ELECOM.2019.05.021**.

153 D. Sun, M. Wang, Z. Li, G. Fan, L. Z. Fan and A. Zhou, Two-dimensional Ti3C2 as anode material for Li-ion batteries, *Electrochem. commun.*, 2014, **47**, 80–83, DOI: **10.1016/J.ELECOM.2014.07.026**.

154 S. Zhao, *et al.*, Li-ion uptake and increase in interlayer spacing of Nb4C3 MXene, *Energy Storage Mater.*, 2017, **8**, 42–48, DOI: **10.1016/J.ENSM.2017.03.012**.

155 C. Wang, S. Chen, H. Xie, S. Wei, C. Wu and L. Song, Ion-Intercalated Layers: Atomic Sn4+ Decorated into Vanadium Carbide MXene Interlayers for Superior Lithium Storage (Adv. Energy Mater. 4/2019), *Adv. Energy Mater.*, 2019, **9**(4), 1970013, DOI: **10.1002/AENM.201970013**.

156 G. Zou, *et al.*, Synthesis of MXene/Ag Composites for Extraordinary Long Cycle Lifetime Lithium Storage at High Rates, *ACS Appl. Mater. Interfaces*, 2016, **8**(34), 22280–22286, DOI: **10.1021/acsami.6b08089**.

157 O. Mashtalir, M. R. Lukatskaya, M. Q. Zhao, M. W. Barsoum and Y. Gogotsi, Amine-assisted delamination of Nb2C MXene

for li-ion energy storage devices, *Adv. Mater.*, 2015, **27**(23), 3501–3506, DOI: **10.1002/adma.201500604**.

158 C. Wei, H. Fei, Y. An, Y. Zhang and J. Feng, Crumpled $Ti_3C_2T_x$ (MXene)nanosheet encapsulated $LiMn_2O_4$ for high performance lithium-ion batteries, *Electrochim. Acta*, 2019, **309**, 362–370, DOI: **10.1016/J.ELECTACTA.2019.04.094**.

159 R. Meng, *et al.*, Black Phosphorus Quantum Dot/Ti_3C_2 MXene Nanosheet Composites for Efficient Electrochemical Lithium/Sodium-Ion Storage, *Adv. Energy Mater.*, 2018, **8**(26), 1801514, DOI: **10.1002/AENM.201801514**.

160 Y. Wang, *et al.*, Fe_3O_4@Ti_3C_2 MXene hybrids with ultra-high volumetric capacity as an anode material for lithium-ion batteries, *J. Mater. Chem. A*, 2018, **6**(24), 11189–11197, DOI: **10.1039/C8TA00122G**.

161 Y. Zhang, *et al.*, MXene/Si@SiO_x@C Layer-by-Layer Super-structure with Autoadjustable Function for Superior Stable Lithium Storage, *ACS Nano*, 2019, **13**(2), 2167–2175, DOI: **10.1021/ACSNANO.8B08821**.

162 G. Zou, *et al.*, Self-reductive synthesis of MXene/$Na_{0.55}Mn_{1.4}$-$Ti_{0.6}O_4$ hybrids for high-performance symmetric lithium ion batteries, *J. Mater. Chem. A*, 2019, **7**(13), 7516–7525, DOI: **10.1039/C9TA00744J**.

163 P. Zhang, D. Wang, Q. Zhu, N. Sun, F. Fu and B. Xu, Plate-to-Layer Bi2MoO6/MXene-Heterostructured Anode for Lithium-Ion Batteries, *Nano-Micro Lett.*, 2019, **11**(1), 81, DOI: **10.1007/S40820-019-0312-Y**.

164 Z. Ma, X. Zhou, W. Deng, D. Lei and Z. Liu, 3D Porous MXene (Ti_3C_2)/Reduced Graphene Oxide Hybrid Films for Advanced Lithium Storage, *ACS Appl. Mater. Interfaces*, 2018, **10**(4), 3634–3643, DOI: **10.1021/acsami.7b17386**.

165 H. Shi, C. J. Zhang, P. Lu, Y. Dong, P. Wen and Z.-S. Wu, Conducting and Lithiophilic MXene/Graphene Framework for High-Capacity, Dendrite-Free Lithium–Metal Anodes, *ACS Nano*, 2019, **13**(12), 14308–14318, DOI: **10.1021/ACSNANO.9B07710**.

166 C. Zhang, A. Wang, J. Zhang, X. Guan, W. Tang and J. Luo, 2D Materials for Lithium/Sodium Metal Anodes, *Adv. Energy Mater.*, 2018, **8**(34), 1802833, DOI: **10.1002/AENM.201802833**.

167 Z. Cao, B. Li and S. Yang, Dendrite-Free Lithium Anodes with Ultra-Deep Stripping and Plating Properties Based on Vertically Oriented Lithium-Copper-Lithium Arrays, *Adv. Mater.*, 2019, **31**(29), 1901310, DOI: **10.1002/ADMA.201901310**.

168 X. Zhang, R. Lv, A. Wang, W. Guo, X. Liu and J. Luo, MXene Aerogel Scaffolds for High-Rate Lithium Metal Anodes, *Angew. Chem., Int. Ed*, 2018, **57**(46), 15028–15033, DOI: **10.1002/ANIE.201808714**.

169 Z. Cao, *et al.*, Perpendicular MXene Arrays with Periodic Interspaces toward Dendrite-Free Lithium Metal Anodes with High-Rate Capabilities, *Adv. Funct. Mater.*, 2020, **30**(5), 1908075, DOI: **10.1002/ADFM.201908075**.

170 Q. Pan, *et al.*, 2D MXene-containing polymer electrolytes for all-solid-state lithium metal batteries, *Nanoscale Adv.*, 2019, **1**(1), 395–402, DOI: **10.1039/C8NA00206A**.

171 X. Liang, A. Garsuch and L. F. Nazar, Sulfur Cathodes Based on Conductive MXene Nanosheets for High-Performance Lithium–Sulfur Batteries, *Angew. Chem., Int. Ed*, 2015, **54**(13), 3907–3911, DOI: **10.1002/ANIE.201410174**.

172 X. Liang, Y. Rangom, C. Y. Kwok, Q. Pang and L. F. Nazar, Interwoven MXene Nanosheet/Carbon-Nanotube Composites as Li–S Cathode Hosts, *Adv. Mater.*, 2017, **29**(3), 1603040, DOI: **10.1002/ADMA.201603040**.

173 Y. V. Mikhaylik and J. R. Akridge, Polysulfide Shuttle Study in the Li/S Battery System, *J. Electrochem. Soc.*, 2004, **151**(11), A1969, DOI: **10.1149/1.1806394**.

174 Y. Fan, K. Liu, A. Ali, X. Chen and P. K. Shen, 2D TiN@C sheets derived from MXene as highly efficient polysulfides traps and catalysts for lithium–sulfur batteries, *Electrochim. Acta*, 2021, **384**, 138187, DOI: **10.1016/J.ELECTACTA.2021.138187**.

175 T. Wang, *et al.*, Hierarchically Porous Ti_3C_2 MXene with Tunable Active Edges and Unsaturated Coordination Bonds for Superior Lithium–Sulfur Batteries, *ACS Nano*, 2021, acsnano.1c06213, DOI: **10.1021/ACSNANO.1C06213**.

176 Z. Ye, Y. Jiang, L. Li, F. Wu and R. Chen, Self-Assembly of 0D–2D Heterostructure Electrocatalyst from MOF and MXene for Boosted Lithium Polysulfide Conversion Reaction, *Adv. Mater.*, 2021, **33**(33), 2101204, DOI: **10.1002/ADMA.202101204**.

177 W. Bao, L. Liu, C. Wang, S. Choi, D. Wang and G. Wang, Facile Synthesis of Crumpled Nitrogen-Doped MXene Nanosheets as a New Sulfur Host for Lithium–Sulfur Batteries, *Adv. Energy Mater.*, 2018, **8**(13), 1702485, DOI: **10.1002/AENM.201702485**.

178 Y. Dong, *et al.*, All-MXene-Based Integrated Electrode Constructed by Ti_3C_2 Nanoribbon Framework Host and Nanosheet Interlayer for High-Energy-Density Li–S Batteries, *ACS Nano*, 2018, **12**(3), 2381–2388, DOI: **10.1021/ACSNANO.7B07672**.

179 C. Wei, *et al.*, Flexible and stable 3D lithium metal anodes based on self-standing MXene/COF frameworks for high-performance lithium-sulfur batteries, *Nano Res.*, 2021, **14**(10), 3576–3584, DOI: **10.1007/S12274-021-3433-9**.

180 Q. Zhu, H. F. Xu, K. Shen, Y. Z. Zhang, B. Li and S. B. Yang, Efficient polysulfides conversion on Mo_2CT_x MXene for high-performance lithium–sulfur batteries, *Rare Met.*, 2021, 1–8, DOI: **10.1007/S12598-021-01839-5**.

181 C. Yao, *et al.*, Properties of *S*-Functionalized Nitrogen-Based MXene (Ti_2NS_2) as a Hosting Material for Lithium–Sulfur Batteries, *Nanomater.*, 2021, **11**(10), 2478, DOI: **10.3390/NANO11102478**.

182 Y. H. Liu, C. Y. Wang, S. L. Yang, F. F. Cao and H. Ye, 3D MXene architectures as sulfur hosts for high-performance lithium-sulfur batteries, *J. Energy Chem.*, 2022, **66**, 429–439, DOI: **10.1016/J.JECHEM.2021.08.040**.

183 D. Xiong, *et al.*, Porosity Engineering of MXene Membrane towards Polysulfide Inhibition and Fast Lithium Ion Transportation for Lithium–Sulfur Batteries, *Small*, 2021, **17**(34), 2007442, DOI: **10.1002/SMLL.202007442**.

184 K.-N. Jung, J. Kim, Y. Yamauchi, M.-S. Park, J.-W. Lee and J. H. Kim, Rechargeable lithium–air batteries: a perspective on the development of oxygen electrodes, *J. Mater. Chem. A*, 2016, **4**(37), 14050–14068, DOI: **10.1039/C6TA04510C**.

185 S. Zhang, G. Wang, J. Jin, L. Zhang and Z. Wen, Coupling solid and soluble catalysts toward stable Li anode for high-performance Li–O$_2$ batteries, *Energy Storage Mater.*, 2020, **28**, 342–349, DOI: **10.1016/J.ENSM.2020.03.018**.

186 G. Girishkumar, B. McCloskey, A. C. Luntz, S. Swanson and W. Wilcke, Lithium–Air Battery: Promise and Challenges, *J. Phys. Chem. Lett.*, 2010, **1**(14), 2193–2203, DOI: **10.1021/JZ1005384**.

187 B. Kumar and J. Kumar, A Solid-State, Rechargeable Lithium Oxygen Battery, *Lithium Air Batter. Fundam*, 2014, **9781489980**, 235–254, DOI: **10.1007/978-1-4899-8062-5_9**.

188 H. Wang, *et al.*, Porous Materials Applied in Nonaqueous Li–O$_2$ Batteries: Status and Perspectives, *Adv. Mater.*, 2020, **32**(44), 2002559, DOI: **10.1002/ADMA.202002559**.

189 S. Yang, P. He and H. Zhou, Research progresses on materials and electrode design towards key challenges of Li–air batteries, *Energy Storage Mater.*, 2018, **13**, 29–48, DOI: **10.1016/J.ENSM.2017.12.020**.

190 M. Wu, *et al.*, Formation of toroidal Li$_2$O$_2$ in non-aqueous Li–O$_2$ batteries with Mo$_2$CT$_x$ MXene/CNT composite, *RSC Adv*, 2019, **9**(70), 41120–41125, DOI: **10.1039/C9RA07699A**.

191 R. Zheng, *et al.*, In Situ Fabricating Oxygen Vacancy-Rich TiO$_2$ Nanoparticles via Utilizing Thermodynamically Meta-stable Ti Atoms on Ti$_3$C$_2$T$_x$ MXene Nanosheet Surface To Boost Electrocatalytic Activity for High-Performance Li–O$_2$ Batteries, *ACS Appl. Mater. Interfaces*, 2019, **11**(50), 46696–46704, DOI: **10.1021/ACSAMI.9B14783**.

192 A. Ahmadiparidari, *et al.*, Enhancing the performance of lithium oxygen batteries through combining redox mediating salts with a lithium protecting salt, *J. Power Sources*, 2021, **491**, 229506, DOI: **10.1016/J.JPOWSOUR.2021.229506**.

193 X. D. Lin, *et al.*, An oxygen-blocking oriented multifunctional solid–electrolyte interphase as a protective layer for a lithium metal anode in lithium–oxygen batteries, *Energy Environ. Sci.*, 2021, **14**(3), 1439–1448, DOI: **10.1039/D0EE02931A**.

194 J. Li, *et al.*, Polarized nucleation and efficient decomposition of Li$_2$O$_2$ for Ti$_2$C MXene cathode catalyst under a mixed surface condition in lithium-oxygen batteries, *Energy Storage Mater.*, 2021, **35**, 669–678, DOI: **10.1016/J.ENSM.2020.12.004**.

195 Q. Zhao, Q. Zhu, J. Miao, P. Zhang and B. Xu, 2D MXene nanosheets enable small-sulfur electrodes to be flexible for lithium–sulfur batteries, *Nanoscale*, 2019, **11**(17), 8442–8448, DOI: **10.1039/C8NR09653H**.

196 H. Tang, *et al.*, A Robust, Freestanding MXene-Sulfur Conductive Paper for Long-Lifetime Li–S Batteries, *Adv. Funct. Mater.*, 2019, **29**(30), 1901907, DOI: **10.1002/ADFM.201901907**.

197 C. Xiong, G. Y. Zhu, H. R. Jiang, Q. Chen and T. S. Zhao, Achieving multiplexed functionality in a hierarchical MXene-based sulfur host for high-rate, high-loading lithium-sulfur batteries, *Energy Storage Mater.*, 2020, **33**, 147–157, DOI: **10.1016/J.ENSM.2020.08.006**.

198 Y. Zhang, *et al.*, An N-doped porous carbon/MXene composite as a sulfur host for lithium–sulfur batteries, *Inorg.*

Chem. Front., 2019, **6**(10), 2894–2899, DOI: **10.1039/C9QI00723G**.

199 L. Jiao, *et al.*, Capture and Catalytic Conversion of Poly-sulfides by In Situ Built TiO$_2$-MXene Heterostructures for Lithium–Sulfur Batteries, *Adv. Energy Mater.*, 2019, **9**(19), 1900219, DOI: **10.1002/AENM.201900219**.

200 D. Zhang, *et al.*, Catalytic Conversion of Polysulfides on Single Atom Zinc Implanted MXene toward High-Rate Lithium–Sulfur Batteries, *Adv. Funct. Mater.*, 2020, **30**(30), 2002471, DOI: **10.1002/ADFM.202002471**.

201 W. Bao, *et al.*, Confined Sulfur in 3D MXene/Reduced Graphene Oxide Hybrid Nanosheets for Lithium–Sulfur Battery, *Chem. – Eur. J.*, 2017, **23**(51), 12613–12619, DOI: **10.1002/CHEM.201702387**.

202 C. Du, J. Wu, P. Yang, S. Li, J. Xu and K. Song, Embedding S@TiO$_2$ nanospheres into MXene layers as high rate cyclability cathodes for lithium–sulfur batteries, *Electro-chim. Acta*, 2019, **295**, 1067–1074, DOI: **10.1016/J.ELECTACTA.2018.11.143**.

203 J. Song, *et al.*, Immobilizing Polysulfides with MXene-Functionalized Separators for Stable Lithium–Sulfur Bat-teries, *ACS Appl. Mater. Interfaces*, 2016, **8**(43), 29427–29433, DOI: **10.1021/acsami.6b09027**.

204 N. Li, W. Cao, Y. Liu, H. Ye and K. Han, Impeding polysulfide shuttling with a three-dimensional conduc-tive carbon nanotubes/MXene framework modified separator for highly efficient lithium-sulfur batteries, *Colloids Surf., A*, 2019, **573**, 128–136, DOI: **10.1016/J.COLSURFA.2019.04.054**.

205 H. Tang, *et al.*, In Situ Formed Protective Barrier Enabled by Sulfur@Titanium Carbide (MXene) Ink for Achieving High-Capacity, Long Lifetime Li-S Batteries, *Adv. Sci.*, 2018, **5**(9), 1800502, DOI: **10.1002/ADVS.201800502**.

206 G. Jiang, *et al.*, In-situ decoration of MOF-derived carbon on nitrogen-doped ultrathin MXene nanosheets to multi-functionalize separators for stable Li–S batteries, *Chem. Eng. J.*, 2019, **373**, 1309–1318, DOI: **10.1016/J.CEJ.2019.05.119**.

207 J. Wang, *et al.*, Laminar MXene-Nafion-modified separator with highly inhibited shuttle effect for long-life lithium–sulfur batteries, *Electrochim. Acta*, 2019, **320**, 134558, DOI: **10.1016/J.ELECTACTA.2019.134558**.

208 Z. Chen, *et al.*, Lithium-Ion-Engineered Interlayers of V2C MXene as Advanced Host for Flexible Sulfur Cathode with Enhanced Rate Performance, *J. Phys. Chem. Lett.*, 2020, **11**(3), 885–890, DOI: **10.1021/acs.jpclett.9b03827**.

209 D. Guo, *et al.*, MXene based self-assembled cathode and antifouling separator for high-rate and dendrite-inhibited Li–S battery, *Nano Energy*, 2019, **61**, 478–485, DOI: **10.1016/J.NANOEN.2019.05.011**.

210 L. Yin, G. Xu, P. Nie, H. Dou and X. Zhang, MXene debris modified eggshell membrane as separator for high-performance lithium-sulfur batteries, *Chem. Eng. J.*, 2018, **352**, 695–703, DOI: **10.1016/J.CEJ.2018.07.063**.

211 Y. Zhang, *et al.*, Rational Design of MXene/1T-2H MoS$_2$-C Nanohybrids for High-Performance Lithium–Sulfur Batteries,

Adv. Funct. Mater., 2018, **28**(38), 1707578, DOI: **10.1002/ ADFM.201707578**.

212 C. Wen, X. Zheng, X. Li, M. Yuan, H. Li and G. Sun, Rational design of 3D hierarchical MXene@AlF3/Ni(OH)$_2$ nanohybrid for high-performance lithium–sulfur batteries, *Chem. Eng. J.*, 2021, **409**, 128102, DOI: **10.1016/J.CEJ.2020.128102**.

213 Z. Wang, X. Li, C. Xuan, J. Li, Y. Jiang and J. Xiao, Photo-synergetic nitrogen-doped MXene/reduced graphene oxide sandwich-like architecture for high-performance lithium-sulfur batteries, *Int. J. Energy Res*, 2021, **45**(2), 2728–2738, DOI: **10.1002/ER.5965**.

214 L. W. Lin, *et al.*, Crumpled nitrogen-doped aerogels derived from MXene and pyrrole-formaldehyde as modified separators for stable lithium-sulfur batteries, *Appl. Surf. Sci.*, 2021, **555**, 149717, DOI: **10.1016/J.APSUSC.2021.149717**.

215 C. Wen, D. Guo, X. Zheng, H. Li and G. Sun, Hierarchical nMOF-867/MXene Nanocomposite for Chemical Adsorption of Polysulfides in Lithium–Sulfur Batteries, *ACS Appl. Energy Mater.*, 2021, **4**(8), 8231–8241, DOI: **10.1021/acsaem.1c01481**.

216 H. Li, *et al.*, Graphene/MXene fibers-enveloped sulfur cathodes for high-performance Li–S batteries, *Electrochim. Acta*, 2021, **371**, 137838, DOI: **10.1016/J.ELECTACTA.2021.137838**.

217 C. Xue, C. Yue and L. Yuan, A simple, robust and fast method for embedding sulfur nanoparticles in Ti$_3$C$_2$T$_x$ MXene as stable lithium–sulfur batteries cathodes, *J. Alloys Compd.*, 2021, **886**, 161152, DOI: **10.1016/ J.JALLCOM.2021.161152**.

218 X. Geng, *et al.*, A Ti$_3$C$_2$T$_x$ MXene - carbon nanocage - sulfur cathode with high conductivity for improving the performance of Li–S batteries, *J. Alloys Compd.*, 2022, **895**, 162586, DOI: **10.1016/J.JALLCOM.2021.162586**.

219 H. Wang, *et al.*, Enhanced kinetics and efficient activation of sulfur by ultrathin MXene coating S-CNTs porous sphere for highly stable and fast charging lithium-sulfur batteries, *Chem. Eng. J.*, 2021, **420**, 129693, DOI: **10.1016/ J.CEJ.2021.129693**.

220 X. Li, C. Wen, H. Li and G. Sun, In situ decoration of nanosized metal oxide on highly conductive MXene nanosheets as efficient catalyst for Li–O$_2$ battery, *J. Energy Chem.*, 2020, **47**, 272–280, DOI: **10.1016/ J.JECHEM.2020.02.016**.

221 X. Li, *et al.*, Nickel oxide nanoparticles decorated highly conductive Ti$_3$C$_2$ MXene as cathode catalyst for rechargeable Li–O$_2$ battery, *J. Alloys Compd.*, 2020, **824**, 153803, DOI: **10.1016/J.JALLCOM.2020.153803**.

222 Z. Sun, *et al.*, Perovskite La$_{0.5}$Sr$_{0.5}$CoO$_{3-\delta}$ Grown on Ti$_3$C$_2$T$_x$ MXene Nanosheets as Bifunctional Efficient Hybrid Catalysts for Li-Oxygen Batteries, *ACS Appl. Energy Mater.*, 2019, **2**(6), 4144–4150, DOI: **10.1021/ACSAEM.9B00328/SUP-PL_FILE/AE9B00328_SI_001.PDF**.

223 G. Li, *et al.*, Highly Efficient Nb2C MXene Cathode Catalyst with Uniform O-Terminated Surface for Lithium–Oxygen Batteries, *Adv. Energy Mater.*, 2021, **11**(1), 2002721, DOI: **10.1002/AENM.202002721**.

224 D. Dall'Agnese, P. L. Taberna, Y. Gogotsi and P. Simon, Two-Dimensional Vanadium Carbide (MXene) as Positive Electrode for Sodium-Ion Capacitors, *J. Phys. Chem. Lett.*, 2015, **6**(12), 2305–2309, DOI: **10.1021/ACS.JPCLETT.5B00868**.

225 X. Wang, *et al.*, Pseudocapacitance of MXene nanosheets for high-power sodium-ion hybrid capacitors, *Nat. Commun.*, 2015, **6**(1), 1–6, DOI: **10.1038/ncomms7544**.

226 X. Wang, X. Shen, Y. Gao, Z. Wang, R. Yu and L. Chen, Atomic-Scale Recognition of Surface Structure and Intercalation Mechanism of Ti$_3$C$_2$X, *J. Am. Chem. Soc.*, 2015, **137**(7), 2715–2721, DOI: **10.1021/JA512820K**.

227 C. Shi, M. Beidaghi, M. Naguib, O. Mashtalir, Y. Gogotsi and S. J. Billinge, Structure of nanocrystalline Ti$_3$C$_2$ MXene using atomic pair distribution function, *Phys. Rev. Lett.*, 2014, **112**, 12, DOI: **10.1103/PHYSREVLETT.112.125501**.

228 Y.-X. Yu, Prediction of Mobility, Enhanced Storage Capacity, and Volume Change during Sodiation on Interlayer-Expanded Functionalized Ti$_3$C$_2$ MXene Anode Materials for Sodium-Ion Batteries, *J. Phys. Chem. C*, 2016, **120**(10), 5288–5296, DOI: **10.1021/ACS.JPCC.5B10366**.

229 Q. Meng, *et al.*, The S-functionalized Ti$_3$C$_2$ Mxene as a high capacity electrode material for Na-ion batteries: a DFT study, *Nanoscale*, 2018, **10**(7), 3385–3392, DOI: **10.1039/ C7NR07649E**.

230 J. Li, *et al.*, Improved sodium-ion storage performance of Ti$_3$C$_2$T$_x$ MXenes by sulfur doping, *J. Mater. Chem. A*, 2018, **6**(3), 1234–1243, DOI: **10.1039/C7TA08261D**.

231 J. Zhu, *et al.*, Two-Dimensional Titanium Carbonitride Mxene for High-Performance Sodium Ion Batteries, *ACS Appl. Nano Mater.*, 2018, **1**(12), 6854–6863, DOI: **10.1021/ ACSANM.8B01330**.

232 J. Luo, *et al.*, Tunable pseudocapacitance storage of MXene by cation pillaring for high performance sodium-ion capacitors, *J. Mater. Chem. A*, 2018, **6**(17), 7794–7806, DOI: **10.1039/C8TA02068J**.

233 X. Xie, K. Kretschmer, B. Anasori, B. Sun, G. Wang and Y. Gogotsi, Porous Ti$_3$C$_2$T$_x$ MXene for Ultrahigh-Rate Sodium-Ion Storage with Long Cycle Life, *ACS Appl. Nano Mater.*, 2018, **1**(2), 505–511, DOI: **10.1021/ACSANM.8B00045**.

234 M.-Q. Zhao, *et al.*, Hollow MXene Spheres and 3D Macroporous MXene Frameworks for Na-Ion Storage, *Adv. Mater.*, 2017, **29**(37), 1702410, DOI: **10.1002/ADMA.201702410**.

235 X. Guo, J. Zhang, J. Song, W. Wu, H. Liu and G. Wang, MXene encapsulated titanium oxide nanospheres for ultra-stable and fast sodium storage, *Energy Storage Mater.*, 2018, **14**, 306–313, DOI: **10.1016/j.ensm.2018.05.010**.

236 C.-F. Du, Q. Liang, Y. Zheng, Y. Luo, H. Mao and Q. Yan, Porous MXene Frameworks Support Pyrite Nanodots toward High-Rate Pseudocapacitive Li/Na-Ion Storage, *ACS Appl. Mater. Interfaces*, 2018, **10**(40), 33779–33784, DOI: **10.1021/ACSAMI.8B13750**.

237 X. Xie, *et al.*, Porous heterostructured MXene/carbon nanotube composite paper with high volumetric capacity for sodium-based energy storage devices, *Nano Energy*, 2016, **26**, 513–523, DOI: **10.1016/J.NANOEN.2016.06.005**.

238 Y. Wu, P. Nie, J. Jiang, B. Ding, H. Dou and X. Zhang, MoS$_2$-Nanosheet-Decorated 2D Titanium Carbide (MXene) as High-Performance Anodes for Sodium-Ion Batteries,

ChemElectroChem, 2017, **4**(6), 1560–1565, DOI: **10.1002/CELC.201700060**.

239 J. Luo, *et al.*, Pillared MXene with Ultralarge Interlayer Spacing as a Stable Matrix for High Performance Sodium Metal Anodes, *Adv. Funct. Mater.*, 2019, **29**(3), 1805946, DOI: **10.1002/ADFM.201805946**.

240 C. Zhang, *et al.*, Potassium Prussian Blue Nanoparticles: A Low-Cost Cathode Material for Potassium-Ion Batteries, *Adv. Funct. Mater.*, 2017, **27**(4), 1604307, DOI: **10.1002/ADFM.201604307**.

241 M. Naguib, *et al.*, Electrochemical performance of MXenes as K-ion battery anodes, *Chem. Commun.*, 2017, **53**(51), 6883–6886, DOI: **10.1039/C7CC02026K**.

242 F. Ming, *et al.*, Porous MXenes enable high performance potassium ion capacitors, *Nano Energy*, 2019, **62**, 853–860, DOI: **10.1016/J.NANOEN.2019.06.013**.

243 P. Lian, *et al.*, Alkalized Ti_3C_2 MXene nanoribbons with expanded interlayer spacing for high-capacity sodium and potassium ion batteries, *Nano Energy*, 2017, **40**, 1–8, DOI: **10.1016/j.nanoen.2017.08.002**.

244 Y. Dong, *et al.*, Ti_3C_2 MXene-Derived Sodium/Potassium Titanate Nanoribbons for High-Performance Sodium/Potassium Ion Batteries with Enhanced Capacities, *ACS Nano*, 2017, **11**(5), 4792–4800, DOI: **10.1021/ACSNANO.7B01165**.

245 H. Huang, J. Cui, G. Liu, R. Bi and L. Zhang, Carbon-Coated $MoSe_2$/MXene Hybrid Nanosheets for Superior Potassium Storage, *ACS Nano*, 2019, **13**(3), 3448–3456, DOI: **10.1021/ACSNANO.8B09548**.

246 X. Tang, *et al.*, MXene-Based Dendrite-Free Potassium Metal Batteries, *Adv. Mater.*, 2020, **32**(4), 1906739, DOI: **10.1002/ADMA.201906739**.

247 Z. Sun, *et al.*, Microbe-assisted assembly of $Ti_3C_2T_x$ MXene on fungi-derived nanoribbon heterostructures for ultra-stable sodium and potassium ion storage, *ACS Nano*, 2021, **15**(2), 3423–3433, DOI: **10.1021/acsnano.0c10491**.

248 M. M. Huie, D. C. Bock, E. S. Takeuchi, A. C. Marschilok and K. J. Takeuchi, Cathode materials for magnesium and magnesium-ion based batteries, *Coord. Chem. Rev.*, 2015, **287**, 15–27, DOI: **10.1016/J.CCR.2014.11.005**.

249 A. Djire, A. Bos, J. Liu, H. Zhang, E. M. Miller and N. R. Neale, Pseudocapacitive Storage in Nanolayered Ti_2NTx MXene Using Mg-Ion Electrolyte, *ACS Appl. Nano Mater*, 2019, **2**(5), 2785–2795, DOI: **10.1021/ACSANM.9B00289**.

250 M. Q. Zhao, C. E. Ren, M. Alhabeb, B. Anasori, M. W. Barsoum and Y. Gogotsi, Magnesium-Ion Storage Capability of MXenes, *ACS Appl. Energy Mater.*, 2019, **2**(2), 1572–1578, DOI: **10.1021/acsaem.8b02253**.

251 F. Liu, Y. Liu, X. Zhao, X. Liu and L.-Z. Fan, Pursuit of a high-capacity and long-life Mg-storage cathode by tailoring sandwich-structured MXene@carbon nanosphere composites, *J. Mater. Chem. A*, 2019, **7**(28), 16712–16719, DOI: **10.1039/C9TA02212K**.

252 M. Xu, N. Bai, H. X. Li, C. Hu, J. Qi and X. Bin Yan, Synthesis of MXene-supported layered MoS_2 with enhanced electrochemical performance for Mg batteries, *Chin. Chem. Lett.*, 2018, **29**(8), 1313–1316, DOI: **10.1016/J.CCLET.2018.04.023**.

253 J. He, *et al.*, Anti-oxidized electrostatic self-assembly of 3D high-density Polyimide@MXene composite for superior aqueous Mg^{2+} storage, *Composites, Part B*, 2021, **222**, 109073, DOI: **10.1016/J.COMPOSITESB.2021.109073**.

254 A. Ponrouch and M. R. Palacin, On the road toward calcium-based batteries, *Curr. Opin. Electrochem.*, 2018, **9**, 1–7, DOI: **10.1016/J.COELEC.2018.02.001**.

255 D. Zhao, *et al.*, Alkali-induced 3D crinkled porous Ti_3C_2 MXene architectures coupled with NiCoP bimetallic phosphide nanoparticles as anodes for high-performance sodium-ion batteries, *Energy Environ. Sci.*, 2019, **12**(8), 2422–2432, DOI: **10.1039/C9EE00308H**.

256 V. Natu, M. Clites, E. Pomerantseva and M. W. Barsoum, Mesoporous MXene powders synthesized by acid induced crumpling and their use as Na-ion battery anodes, *Mater. Res. Lett.*, 2018, **6**(4), 230–235, DOI: **10.1080/21663831.2018.1434249**.

257 Y. Wu, P. Nie, J. Wang, H. Dou and X. Zhang, Few-Layer MXenes Delaminated via High-Energy Mechanical Milling for Enhanced Sodium-Ion Batteries Performance, *ACS Appl. Mater. Interfaces*, 2017, **9**(45), 39610–39617, DOI: **10.1021/acsami.7b12155**.

258 Y. Wu, P. Nie, L. Wu, H. Dou and X. Zhang, 2D MXene/SnS_2 composites as high-performance anodes for sodium ion batteries, *undefined*, 2018, **334**, 932–938, DOI: **10.1016/J.CEJ.2017.10.007**.

259 F. Wu, *et al.*, A 3D flower-like VO_2/MXene hybrid architecture with superior anode performance for sodium ion batteries, *J. Mater. Chem. A*, 2019, **7**(3), 1315–1322, DOI: **10.1039/C8TA11419F**.

260 S. Sun, Z. Xie, Y. Yan and S. Wu, Hybrid energy storage mechanisms for sulfur-decorated Ti_3C_2 MXene anode material for high-rate and long-life sodium-ion batteries, *Chem. Eng. J.*, 2019, **366**, 460–467, DOI: **10.1016/J.CEJ.2019.01.185**.

261 R. Zhao, *et al.*, Molecular-level heterostructures assembled from layered black phosphorene and Ti_3C_2 MXene as superior anodes for high-performance sodium ion batteries, *Nano Energy*, 2019, **366**, 460–467, DOI: **10.1016/J.NANOEN.2019.104037**.

262 X. Guo, *et al.*, Sb_2O_3/MXene($Ti_3C_2T_x$) hybrid anode materials with enhanced performance for sodium-ion batteries, *J. Mater. Chem. A*, 2017, **5**(24), 12445–12452, DOI: **10.1039/C7TA02689G**.

263 Q. Yang, *et al.*, A synergistic Bi2S3/MXene composite with enhanced performance as an anode material of sodium-ion batteries, *New J. Chem.*, 2020, **44**(7), 3072–3077, DOI: **10.1039/C9NJ05986E**.

264 Z. Hu, Q. Liu, S. L. Chou and S. X. Dou, Two-Dimensional Material-Based Heterostructures for Rechargeable Batteries, *Cell Rep. Phys. Sci.*, 2021, **2**(1), 1–19, DOI: **10.1016/j.xcrp.2020.100286**.

265 Z. Li, *et al.*, Coupling of ReS_2 nanosheet arrays with hollow $NiCoS_4$ nanocubes enables ultrafast Na^+ diffusion kinetics

and super Na$^+$ storage of a NiCoS$_4$@ReS$_2$ heterostructure, *Mater. Chem. Front*, 2021, **5**(20), 7540–7547, DOI: **10.1039/D1QM00841B**.

266 W. Zhang, *et al.*, Wasp nest-imitated assembly of elastic rGO/p-Ti$_3$C$_2$T$_x$ MXene-cellulose nanofibers for high-performance sodium-ion batteries, *Carbon N. Y*, 2019, **153**, 625–633, DOI: **10.1016/J.CARBON.2019.07.040**.

267 X. Wang, *et al.*, Ultrafine ZnSe Encapsulated in Nitrogen-Doped Porous Carbon Nanofibers for Superior Na-Ion Batteries with a Long Lifespan and Low-Temperature Performance, *ACS Sustain. Chem. Eng.*, 2021, **9**(35), 11705–11713, DOI: **10.1021/acssuschemeng.1c02447**.

268 E. Xu, *et al.*, Dimensional Gradient Structure of CoSe$_2$@CNTs–MXene Anode Assisted by Ether for High-Capacity, Stable Sodium Storage, *Nano-Micro Lett.*, 2021, **13**(1), 40, DOI: **10.1007/S40820-020-00562-7**.

269 M. Q. Zhao, N. Trainor, C. E. Ren, M. Torelli, B. Anasori and Y. Gogotsi, Scalable Manufacturing of Large and Flexible Sheets of MXene/Graphene Heterostructures, *Adv. Mater. Technol.*, 2019, **4**(5), 1800639, DOI: **10.1002/ADMT.201800639**.

270 J. Huang, *et al.*, Sandwich-like Na$_{0.23}$TiO$_2$ nanobelt/Ti$_3$C$_2$ MXene composites from a scalable in situ transformation reaction for long-life high-rate lithium/sodium-ion batteries, *Nano Energy*, 2018, **46**, 20–28, DOI: **10.1016/J.NANOEN.2018.01.030**.

271 H. Wang, *et al.*, Interfacial Covalent Bonding Endowing Ti$_3$C$_2$-Sb$_2$S$_3$ Composites High Sodium Storage Performance, *Small*, 2021, 2104293, DOI: **10.1002/SMLL.202104293**.

272 R. Zhao, *et al.*, Self-assembled Ti$_3$C$_2$ MXene and N-rich porous carbon hybrids as superior anodes for high-performance potassium-ion batteries, *Energy Environ. Sci.*, 2020, **13**(1), 246–257, DOI: **10.1039/C9EE03250A**.

273 W. Kang, Y. Wang and C. An, Interlayer engineering of MoS$_2$ nanosheets for high-rate potassium-ion storage, *New J. Chem.*, 2020, **44**(47), 20659–20664, DOI: **10.1039/D0NJ04314A**.

274 G. Ma, Y. Zhou, Y. Wang, Z. Feng and J. Yang, N,P-codoped graphene supported few-layered MoS$_2$ as a long-life and high-rate anode materials for potassium-ion storage, *Nano Res.*, 2021, **14**(10), 3523–3530, DOI: **10.1007/S12274-021-3606-6**.

275 Y. Tian, Y. An, S. Xiong, J. Feng and Y. Qian, A general method for constructing robust, flexible and freestanding MXene@metal anodes for high-performance potassium-ion batteries, *J. Mater. Chem. A*, 2019, **7**(16), 9716–9725, DOI: **10.1039/C9TA02233C**.

276 Y. Cao, *et al.*, SnS$_2$ Nanosheets Anchored on Nitrogen and Sulfur Co-Doped MXene Sheets for High-Performance Potassium-Ion Batteries, *ACS Appl. Mater. Interfaces*, 2021, **13**(15), 17668–17676, DOI: **10.1021/acsami.1c02590**.

277 J. Cao, *et al.*, Ti$_3$C$_2$T$_x$ MXene Conductive Layers Supported Bio-Derived Fe$_{x-1}$Se$_x$/MXene/Carbonaceous Nanoribbons for High-Performance Half/Full Sodium-Ion and Potassium-Ion Batteries, *Adv. Mater.*, 2021, **33**(34), 2101535, DOI: **10.1002/ADMA.202101535**.

278 N. Sun, *et al.*, MXene-Bonded Flexible Hard Carbon Film as Anode for Stable Na/K-Ion Storage, *Adv. Funct. Mater.*, 2019, **29**(51), 1906282, DOI: **10.1002/ADFM.201906282**.

279 X. Wu, H. Wang, Z. Zhao and B. Huang, Interstratification-assembled 2D black phosphorene and V$_2$CT$_x$ MXene as superior anodes for boosting potassium-ion storage, *J. Mater. Chem. A*, 2020, **8**(25), 12705–12715, DOI: **10.1039/D0TA04506C**.

280 Z. Xia, *et al.*, Designing N-doped graphene/ReSe$_2$/Ti$_3$C$_2$ MXene heterostructure frameworks as promising anodes for high-rate potassium-ion batteries, *J. Energy Chem.*, 2020, **53**, 155–162, DOI: **10.1016/J.JECHEM.2020.04.071**.

281 Y. Li, D. Xu, D. Zhang, Y. Wei, R. Zhang and Y. Guo, Study on MnO$_2$/MXene–Ti$_3$C$_2$ composite materials as cathode materials for magnesium batteries, *RSC Adv*, 2019, **9**(58), 33572–33577, DOI: **10.1039/C9RA07652B**.

282 M. Xu, *et al.*, Opening Magnesium Storage Capability of Two-Dimensional MXene by Intercalation of Cationic Surfactant, *ACS Nano*, 2018, **12**(4), 3733–3740, DOI: **10.1021/acsnano.8b00959**.

283 A. Byeon, *et al.*, Two-Dimensional Titanium Carbide MXene As a Cathode Material for Hybrid Magnesium/Lithium-Ion Batteries, *ACS Appl. Mater. Interfaces*, 2017, **9**(5), 4296–4300, DOI: **10.1021/ACSAMI.6B04198**.

284 D. Zhang, S. Wang, B. Li, Y. Gong and S. Yang, Horizontal Growth of Lithium on Parallelly Aligned MXene Layers towards Dendrite-Free Metallic Lithium Anodes, *Adv. Mater.*, 2019, **31**, 33, DOI: **10.1002/ADMA.201901820**.

285 H. Shi, *et al.*, 3D Flexible, Conductive, and Recyclable Ti$_3$C$_2$T$_x$ MXene-Melamine Foam for High-Areal-Capacity and Long-Lifetime Alkali-Metal Anode, *ACS Nano*, 2020, **14**(7), 8678–8688, DOI: **10.1021/ACSNANO.0C03042**.

286 C. Y. Wang, Z. J. Zheng, Y. Q. Feng, H. Ye, F. F. Cao and Z. P. Guo, Topological design of ultrastrong MXene paper hosted Li enables ultrathin and fully flexible lithium metal batteries, *Nano Energy*, 2020, **74**, 104817, DOI: **10.1016/J.NANOEN.2020.104817**.

287 J. Gu, *et al.*, Single Zinc Atoms Immobilized on MXene (Ti$_3$C$_2$Clx) Layers toward Dendrite-Free Lithium Metal Anodes, *ACS Nano*, 2020, **14**(1), 891–898, DOI: **10.1021/acsnano.9b08141**.

288 Y. An, *et al.*, Porosity- and Graphitization-Controlled Fabrication of Nanoporous Silicon@Carbon for Lithium Storage and Its Conjugation with MXene for Lithium-Metal Anode, *Adv. Funct. Mater.*, 2020, **30**(9), 1908721, DOI: **10.1002/ADFM.201908721**.

289 K. Shen, B. Li and S. Yang, 3D printing dendrite-free lithium anodes based on the nucleated MXene arrays, *Energy Storage Mater.*, 2020, **24**, 670–675, DOI: **10.1016/J.ENSM.2019.08.015**.

290 C. Xiong, Z. Wang, X. Peng, Y. Guo, S. Xu and T. Zhao, Bifunctional effect of laser-induced nucleation-preferable microchannels and: in situ formed LiF SEI in MXenes for stable lithium-metal batteries, *J. Mater. Chem. A*, 2020, **8**(28), 14114–14125, DOI: **10.1039/d0ta04302h**.

291 C. Wei, *et al.*, Isotropic Li nucleation and growth achieved by an amorphous liquid metal nucleation seed on MXene

framework for dendrite-free Li metal anode, *Energy Storage Mater.*, 2020, **26**, 223–233, DOI: **10.1016/J.ENSM.2020.01.005**.

292 Y. Tian, *et al.*, Flexible and Free-Standing $Ti_3C_2T_x$ MXene@Zn Paper for Dendrite-Free Aqueous Zinc Metal Batteries and Nonaqueous Lithium Metal Batteries, *ACS Nano*, 2019, **13**(10), 11676–11685, DOI: **10.1021/acsnano.9b05599**.

293 Y. Tian, *et al.*, Stable and dendrite-free lithium metal anodes enabled by carbon paper incorporated with ultra-fine lithiophilic TiO_2 derived from MXene and carbon dioxide, *Chem. Eng. J.*, 2021, **406**, 126836, DOI: **10.1016/J.CEJ.2020.126836**.

294 J. Wang, M. Yang, G. Zou, D. Liu and Q. Peng, Lithiation MXene Derivative Skeletons for Wide-Temperature Lithium Metal Anodes, *Adv. Funct. Mater.*, 2021, **31**(21), 2101180, DOI: **10.1002/ADFM.202101180**.

295 X. Qian, *et al.*, Polysiloxane Cross-Linked Mechanically Stable MXene-Based Lithium Host for Ultrastable Lithium Metal Anodes with Ultrahigh Current Densities and Capacities, *Adv. Funct. Mater.*, 2021, **31**(6), 2008044, DOI: **10.1002/ADFM.202008044**.

296 X. He, *et al.*, A 3D Hydroxylated MXene/Carbon Nanotubes Composite as a Scaffold for Dendrite-Free Sodium-Metal Electrodes, *Angew. Chemie*, 2020, **59**(38), 16705–16711, DOI: **10.1002/ANGE.202006783**.

297 Y. Fang, *et al.*, Induction of Planar Sodium Growth on MXene $(Ti_3C_2T_x)$-Modified Carbon Cloth Hosts for Flexible Sodium Metal Anodes, *ACS Nano*, 2020, **14**(7), 8744–8753, DOI: **10.1021/ACSNANO.0C03259/SUPPL_FILE/NN0C03259_SI_002.MP4**.

298 J. Luo, *et al.*, Tunable MXene-Derived 1D/2D Hybrid Nanoarchitectures as a Stable Matrix for Dendrite-Free and Ultrahigh Capacity Sodium Metal Anode, *Nano Lett*, 2020, **20**(10), 7700–7708, DOI: **10.1021/acs.nanolett.0c03215**.

299 H. Shi, Y. Dong, S. Zheng, C. Dong and Z. S. Wu, Three dimensional Ti_3C_2 MXene nanoribbon frameworks with uniform potassiophilic sites for the dendrite-free potassium metal anodes, *Nanoscale Adv.*, 2020, **2**(9), 4212–4219, DOI: **10.1039/D0NA00515K**.

300 L. Qin, *et al.*, Capillary Encapsulation of Metallic Potassium in Aligned Carbon Nanotubes for Use as Stable Potassium Metal Anodes, *Adv. Energy Mater.*, 2019, **9**(29), 1901427, DOI: **10.1002/AENM.201901427**.

301 D. Sun, *et al.*, Structural Transformation of MXene (V_2C, Cr_2C, and Ta_2C) with O Groups during Lithiation: A First-Principles Investigation, *ACS Appl. Mater. Interfaces*, 2016, **8**(1), 74–81, DOI: **10.1021/ACSAMI.5B03863/SUPPL_FILE/AM5B03863_SI_001.ZIP**.

302 J. Nan, *et al.*, Nanoengineering of 2D MXene-Based Materials for Energy Storage Applications, *Small*, 2021, **17**(9), 1902085, DOI: **10.1002/SMLL.201902085**.

303 C. (John) Zhang, L. Cui, S. Abdolhosseinzadeh and J. Heier, Two-dimensional MXenes for lithium–sulfur batteries, *InfoMat*, 2020, **2**(4), 613–638, DOI: **10.1002/inf2.12080**.

304 L. Giebeler and J. Balach, MXenes in lithium–sulfur batteries: scratching the surface of a complex 2D material – A minireview, *Mater. Today Commun.*, 2021, **27**, 102323, DOI: **10.1016/j.mtcomm.2021.102323**.

305 Z. Wang, X. Chen, F. Shen, X. Hang and C. Niu, TiC MXene High Energy Density Cathode for Lithium–Air Battery, *Adv. Theory Simul.*, 2018, **1**(9), 1800059, DOI: **10.1002/ADTS.201800059**.

306 H. Shi, C. J. Zhang, P. Lu, Y. Dong, P. Wen and Z. S. Wu, Conducting and Lithiophilic MXene/Graphene Framework for High-Capacity, Dendrite-Free Lithium-Metal Anodes, *ACS Nano*, 2019, **13**(12), 14308–14318, DOI: **10.1021/ACS-NANO.9B07710/SUPPL_FILE/NN9B07710_SI_003.MP4**.

307 X. Meng, Y. Sun, M. Yu, Z. Wang and J. Qiu, Hydrogen-Bonding Crosslinking MXene to Highly Robust and Ultralight Aerogels for Strengthening Lithium Metal Anode, *Small Sci*, 2021, **1**(9), 2100021, DOI: **10.1002/SMSC.202100021**.

308 M. K. Aslam and M. Xu, A Mini-Review: MXene composites for sodium/potassium-ion batteries, *Nanoscale*, 2020, **12**(30), 15993–16007, DOI: **10.1039/d0nr04111d**.

309 P. Ma, D. Fang, Y. Liu, Y. Shang, Y. Shi and H. Y. Yang, MXene-Based Materials for Electrochemical Sodium-Ion Storage, *Adv. Sci*, 2021, **8**(11), 2003185, DOI: **10.1002/ADVS.202003185**.

310 S. Arnold, *et al.*, Design of high-performance antimony/MXene hybrid electrodes for sodium-ion batteries, *J. Mater. Chem. A*, 2022, **10**(19), 10569–10585, DOI: **10.1039/D2TA00542E**.

311 H. Kaland, *et al.*, Are MXenes suitable as cathode materials for rechargeable Mg batteries?, *Sustain. Energy Fuels*, 2020, **4**(6), 2956–2966, DOI: **10.1039/D0SE00087F**.